Charles University, Faculty of Mathematics and Physics
Institute of Theoretical Physics

Dynamic Effects in Weak and Strong Gravitation

habilitation thesis

Tomáš Ledvinka

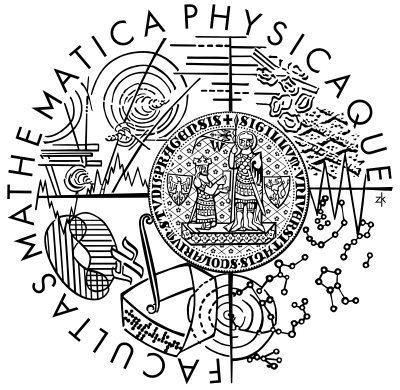

Prague 2021

Acknowledgement

I thank Jiří Bičák for his support and inspiration. The work presented would also not be feasible without the support of my colleagues from the Institute of Theoretical Physics.

My work was partially supported by the Grant Agency of the Czech Republic, Czech Ministry of Education and Collaborative Research Center SFB/TR7 of Federal Republic of Germany.

Introduction

The beautiful Einstein's explanation of the gravitational interaction as a dynamic interplay of the spacetime geometry and the fields spreading in this curved canvas led to enormous theoretical discoveries and surprising explanations of otherwise puzzling observations. The methods developed in the field of general relativity include new approaches to differential geometry, classical field theory, analytic approximation methods, or numerical methods.

The Thesis presents several topics contained in six selected original papers [P1-P6] utilizing these methods. The first topic, *Hamiltonian description of gravitational interaction*, arose from the cooperation of our institute with Friedrich Schiller Universität in Jena and Zentrum für angewandte Raumfahrttechnologie und Mikrogravitation in Bremen. In my studies of *Dragging effects of gravitational waves* I joined the long-term project of Jiří Bičák, Joseph Katz and Donald Lynden-Bell devoted to Machian effects in general relativity. Finally, *Gravitational collapse of gravitational waves* belongs to numerical relativity — the field I brought from my postdoc stay at Universitat de les Illes Balears in Palma de Mallorca. In all of these topics, the dynamics of fields and bodies plays an important role either appearing in the weak field limit or involving extremely strong gravitation fields, all in the context of classical general relativity in 3+1 dimensions:

- In general relativity, an exact treatment of the two-body problem is not available. Various analytic approximation techniques thus have been developed, usually in the form of an expansion in a small parameter, such as velocity of motion, mass ratio of the interacting bodies, or the gravitational constant. In the latter approach, gravitating bodies can move with arbitrary velocity and it is thus called post-Minkowskian (PM) approximation. If no other interaction of the bodies is assumed, the only source of their acceleration is the gravitational interaction, so in the first PM approximation the bodies "feel" only that part of the gravitational field of the other bodies which corresponds to their uniform, unaccelerated motion. This approximation then allows us to remove the field degrees of freedom from the problem and find a closed-form Hamiltonian for a system of gravitationally interacting bodies [P1].

  Since real neutron stars and black holes rotate, the Hamiltonian description of the motion of gravitating spinning bodies plays an essential role in gravitational physics. In a certain (the so-called *pole-dipole*) approximation, a spinning body is represented by a particle endowed with position, momentum, and spin satisfying the respective Poisson-Dirac brackets for such canonical quantities. We show that a certain choice of local coordinate systems leads to a simpler Hamiltonian description of the motion of a spinning test particle in the vicinity of the Kerr black hole [P2].

- Because in general relativity the gravitational field is a tensor field, bodies deform the spacetime not only into simple gravity wells. It is also their motion (momentum) which

is imprinted in the gravitational field and can yield effects similar to those of the thought experiment of Mach who — before Einstein would attribute this property to the gravitational field itself — conjectured that it is perhaps the far-away stars what determines which of the local frames is the nonrotating one.

While the influence of the rotating matter on the gyroscope it surrounds (an effect usually called dragging) is thoroughly studied, the case of gravitational waves is more subtle. In agreement with our elementary spacetime experience, we consider weak gravitational waves in a flat Minkowski spacetime and study their influence on the inertial frame of an observer surrounded even though not exposed to these waves. If the amplitude of the gravitational wave is taken as an expansion parameter, for a particular shape of the rotating gravitational wave packet describing the first-order approximation of a gravitational wave around a Minkowski background, we find explicit formulas for the second-order quantities describing the dragging effects [P3,P4].

- For stronger gravitational waves, the nonlinear effects open the possibility that so much energy is concentrated into a small enough volume that a black hole is formed. This problem must be treated numerically and despite great breakthroughs in numerical relativity, certain aspects of this process are still not understood. To perform such computations, the obvious feature of general relativity — that it is a gauge theory — turns out to be a serious obstacle as the strong dynamic gravitational field cannot be decoupled from the strong dynamics of the coordinates used in the description of the spacetime. The nonlinearities of the theory thus on the one hand imply the existence of black holes and the singularities they contain, and on the other hand these nonlinearities may lead to singular coordinates.

  Apart from an obvious increase of computing power, the breakthroughs made in the 2000s involved understanding how to choose coordinates in highly dynamic spacetimes with collapsing matter or orbiting and merging black holes. But this *moving puncture* method does not work for the collapse of gravitational waves. This makes the formation of black holes by collapse of gravitational waves an important, yet purely theoretical problem. In [P5], we were able to find a recipe for the coordinates numerically constructed during the gravitational wave collapse, which enabled us to follow this process during near-critical gravitational collapse, i.e., in situations where fine-tuned initial data lead to the creation of extremely small black holes. A detailed analysis of these simulations revealed surprising features of a phenomenon sought for for almost three decades — the self-similarity in near-critical spacetimes arising in the collapse of gravitational waves [P6].

Apart from Einstein's theory of gravitation, what these topics have in common is that the presented results were obtained with the help of modern computers. While the last topic belongs to the number-crunching field of numerical relativity, all of them exploit heavily the capabilities of modern *computer algebra* systems which can sometimes reduce very long calculations into tractable resulting formulas.

Contents

Chapter 1

Overview of studied problems

1.1 Hamiltonian description of gravitational interaction

Theoretical physics started as Newtonian mechanics in the 17th century with the notions of gravitation force, point particles, and inertia. In 1827 W. R. Hamilton reformulated this problem in a way which became very useful in celestial mechanics, the true realm of gravity. A very attractive explanation of gravitational interaction where the curved spacetime arena becomes the medium of gravity was then discovered by A. Einstein in 1915. The complicated structure of this theory required application of approximation methods, some of which return to the notion of interacting massive particles. Among others, the so-called post-Newtonian approximation succeeded in predicting the exact behavior of the inspiral phase of black hole and neutron star mergers. These predictions were later confirmed and extended by the results of numerical relativity and evolved into another powerful approximation method, the so-called effective one-body formulation of the binary black hole problem. These theoretical results were then utilized to interpret the observations by the interferometric gravitational wave observatories LIGO and Virgo.

1.1.1 Hamiltonian for many-body gravitating system in the post-Minkowskian approximation

I had an opportunity to join G. Schäfer and J. Bičák and study the Hamiltonian description of an N-body system in the post-Minkowskian (PM) approximation of general relativity [P1]. Unlike the post-Newtonian approximation, which assumes small velocities and uses this velocity as the expansion parameter (which is appropriate for orbiting bodies), the post-Minkowskian approximation uses as the expansion parameter the gravitational interaction constant G. Thus, despite G being equal to 1 in the usual geometrical units, we retain it here so that we can explicitly see how the expansion in G proceeds and we indicate which terms are neglected using Landau's O notation.

Introduction

Variational formulation is an essential feature of the fundamental physical laws. The Einstein-Hilbert action

$$S_{\text{gravity}} = \frac{1}{16\pi G} \int {}^{(4)}R \sqrt{g}\, d^4x, \tag{1.1}$$

where the gravitational field is described by the metric $g_{\mu\nu}(x^\kappa)$; $\mu,\nu = 0,1,2,3$ determining the Ricci curvature scalar ${}^{(4)}R$ and providing the invariant volume element $\sqrt{g}\,d^4x$, seems surprisingly simple and yet it leads to the Einstein equations with all their intricacies.

In the Hamiltonian approach [1], the covariant unification of space and time is abandoned and the so-called 3+1 splitting of the spacetime geometry is used. The time coordinate t defines hypersurfaces $t = \text{const}$ with the unit normal n_μ and the 3-metric of such time-slice represents the dynamical field γ_{ij}, with $i,j = 1,2,3$. The spacetime geometry is then

$$ds^2 = -N^2\,dt^2 + \gamma_{ij}(dx^i - N^i dt)(dx^j - N^j dt), \tag{1.2}$$

where $N(t,x^j)$ and $N^i(t,x^j)$ are metric coefficients (called respectively *lapse* and *shift*) which, rather than being dynamical fields, are related to the choice of coordinates (gauge). If the metric satisfies the Einstein equations $G^{\mu\nu} = 8\pi G\,T^{\mu\nu}$, then the metric γ_{ij} and its momentum π^{ij} must satisfy the so-called Hamilton and momentum constraints

$$\mathcal{H} \equiv \frac{1}{16\pi G}\left[-\gamma^{1/2}R + \frac{1}{\gamma^{1/2}}\left(\gamma_{ik}\gamma_{jl}\pi^{ij}\pi^{kl} - \frac{1}{2}(\gamma_{ij}\pi^{ij})^2\right)\right] + \mathcal{H}^{\text{matter}} = 0, \tag{1.3}$$

$$\mathcal{H}_i \equiv \frac{1}{8\pi G}\gamma_{ij}\nabla_k\pi^{jk} + \mathcal{H}_i^{\text{matter}} = 0, \tag{1.4}$$

where $\mathcal{H}^{\text{matter}} = \sqrt{\gamma}T^{\mu\nu}n_\mu n_\nu$ and $\mathcal{H}_i^{\text{matter}} = -\sqrt{\gamma}T_i{}^\nu n_\nu$ are projected components of the matter stress-energy tensor and ∇_k is a covariant derivative compatible with γ_{ij} whose Ricci curvature scalar is denoted R.

The Hamiltonian theory for constrained systems shows that $N(t,x^j)$ and $N^i(t,x^j)$ play the role of Lagrange multipliers and the Arnowitt-Deser-Misner (ADM) Hamiltonian function for metric and matter reads [2], [3]

$$H[(\gamma_{ij},\pi^{ij})^{\text{gravity}};(q,p)^{\text{matter}}] = \int (N\mathcal{H} - N^i\mathcal{H}_i)d^3x + \frac{1}{16\pi G}\oint_{r\to\infty}\partial_i(\gamma_{ij} - \delta_{ij}\gamma_{kk})dS_j, \tag{1.5}$$

where near the spatial infinity we assume flat Minkowski spatial coordinates x^i, so that $\gamma_{ij} \to \delta_{ij} + O(1/r)$ and similarly for the lapse and shift functions, $\delta_{ij} = \delta^{ij}$ is the Kronecker delta. The solution of the constraint equations is enabled by a decomposition of γ_{ij} and π^{ij} into constrained fields (Φ,π^j) and free transverse-traceless (TT) fields $(h_{ij}^{\text{TT}},\pi_{\text{TT}}^{ij})$

$$\gamma_{ij} = \left(1 + \frac{1}{8}\Phi\right)^4\delta_{ij} + h_{ij}^{\text{TT}}, \tag{1.6}$$

$$\pi^{ij} = \partial_i\pi^j + \partial_j\pi^i - \frac{2}{3}\delta^{ij}\partial_k\pi^k + \pi_{\text{TT}}^{ij}. \tag{1.7}$$

In the so-called ADM gauge $\delta^{jk}(3\gamma_{ij,k} - \gamma_{jk,i}) = 0$ and $\delta_{ij}\pi^{ij} = 0$, the free fields satisfy $h_{ii}^{\text{TT}} = 0$, $h_{ij,j}^{\text{TT}} = 0$ and $\pi_{\text{TT}}^{ii} = 0$. Then the constraint equations can be solved for Φ and π^j. Because near infinity $\partial_i(\gamma_{ij} - \delta_{ij}\gamma_{kk})\,dS_j = -\partial_j\Phi\;dS_j$, with satisfied constraints, (1.5) then (with $\Delta \equiv \partial_{kk}$) simplifies to

$$H[(\gamma_{ij}^{\text{TT}},\pi_{\text{TT}}^{ij})^{\text{gravity}};(q,p)^{\text{matter}}] = -\frac{1}{16\pi G}\int \Delta\Phi\;d^3x. \tag{1.8}$$

Surprisingly, this means that in this approach shift and lapse functions are not needed to determine the evolution of field variables and, as we will see, also that of matter represented

by massive particles. The value of H also provides the so-called ADM mass and application of the Gauss theorem on (1.8) shows the relation between the asymptotic falloff of Φ and ADM mass.

It turns out that (1.8) also determines the matter equations of motion when used as a Hamiltonian for variables formally denoted $q^{\rm matter}$ and $p^{\rm matter}$. Note, that the solution of the constraint equations (1.3) and (1.4) provides the dependence of Φ and π^i and thus also of the ADM mass on the matter variables $q^{\rm matter}$, $p^{\rm matter}$ and field variable $\gamma_{ij}^{\rm TT}, \pi_{\rm TT}^{ij}$. They thus appear as arguments on the left-hand side of (1.8).

Although black holes are extended bodies, the approximation methods based on this approach very successfully use simple positions and momenta $\mathbf{x}_a$ and $\mathbf{p}_a$ and prescribe the stress energy tensor components of the a-th black hole to be proportional to $\overline{m}_a\delta(\mathbf{x}-\mathbf{x}_a)$, where $\overline{m}_a = \sqrt{m_a^2+\mathbf{p}_a^2}$. The simplest argument is based on the observations that for a single "particle" the field Φ satisfying $\Delta\Phi = -16\pi G m\delta(\mathbf{x})$ corresponds to the Schwarzschild black hole spacetime in isotropic coordinates and that a pair of δ-function sources leads to the Brill-Lindquist binary black hole initial data [4]. See [1] for a detailed discussion. The nonlinear constraint equations are then solved using an iterative approach. In our approximation, $\Delta\Phi$ can be simply expressed using the Hamilton constraint (1.3) which after neglecting higher order terms and a total divergence reads

$$\frac{1}{16\pi G}\left[(1+\frac{1}{8}\Phi)\Delta\Phi + \frac{1}{4}h^{\rm TT}_{ij,k}h^{\rm TT}_{ij,k} + \frac{1}{\gamma^{1/2}}\left(\gamma_{ik}\gamma_{jl}\pi^{ij}\pi^{kl} - \frac{1}{2}(\gamma_{ij}\pi^{ij})^2\right)\right] + \sum_a \overline{m}_a\delta^3(\mathbf{x}-\mathbf{x}_a) = 0.$$

Note that leading-order terms of this equation yield $\Delta\Phi \doteq -16\pi G\sum_a \overline{m}_a\delta^3(\mathbf{x}-\mathbf{x}_a)$ and thus $\Phi \doteq 4G\sum_a \overline{m}_a/|\mathbf{x}-\mathbf{x}_a|$. Then the Newtonian gravitational potential term in the Hamiltonian arises from the term $\frac{1}{8}\Phi\,\Delta\Phi$. While in the so-called post-Newtonian (PN) approximation the remaining terms are of a higher order in velocities (or momenta) as well as $\overline{m}_a \doteq m_a + |\mathbf{p}_a|^2/(2m_a) + ...$, in the post-Minkowskian approximation we have to retain the complete relativistic masses $\overline{m}_a$ and all terms proportional to G.

Important steps were made by Schäfer in [5] where the contributions arising from the constrained fields Φ and π^j were found including terms $O(G^2)$. Keeping only terms up to the first order in G, it reads

$$\begin{aligned} H_{\rm lin} = &\sum_a \overline{m}_a - \frac{1}{2}G\sum_{a,b\neq a}\frac{\overline{m}_a\overline{m}_b}{r_{ab}}\left(1+\frac{p_a^2}{\overline{m}_a^2}+\frac{p_b^2}{\overline{m}_b^2}\right) + \frac{1}{4}G\sum_{a,b\neq a}\frac{1}{r_{ab}}\left(7\,\mathbf{p}_a\cdot\mathbf{p}_b + (\mathbf{p}_a\cdot\mathbf{n}_{ab})(\mathbf{p}_b\cdot\mathbf{n}_{ab})\right) \\ &- \frac{1}{2}\sum_a \frac{p_{ai}p_{aj}}{\overline{m}_a}\,h_{ij}^{TT}(\mathbf{x}=\mathbf{x}_a) + \frac{1}{16\pi G}\int d^3x\,\left(\frac{1}{4}h^{TT}_{ij,k}\,h^{TT}_{ij,k} + \pi^{ij\,TT}\pi^{ij\,TT}\right), \end{aligned} \tag{1.9}$$

The first line describes the direct interaction of particles originating in the solution of constraint equations, the second line then contains the interaction term and the free-field Hamiltonian leading to a simple flat-space wave operator. This Hamiltonian enables us to obtain the evolution equations for particles and field in the given approximation — the equations which must be solved simultaneously:

$$\dot{h}_{ij}^{TT} = \delta_{ij}^{TT\,kl}\frac{\delta H}{\delta\bar{\pi}^{kl\,TT}}, \qquad \dot{\bar{\pi}}^{ij\,TT} = -\,\delta_{kl}^{TT\,ij}\frac{\delta H}{\delta h_{kl}^{TT}}, \tag{1.10}$$

$$\dot{\mathbf{x}}_a = \frac{\partial H}{\partial\mathbf{p}_a}, \qquad \dot{\mathbf{p}}_a = -\frac{\partial H}{\partial\mathbf{x}_a}. \tag{1.11}$$

Here we use the exactly canonically conjugated field momenta $\bar{\pi}^{ij\,TT} = (16\pi G)^{-1}\pi^{ij\,TT}$, $\delta H/\delta\psi$ stands for variational derivative and we also use the TT-projection operator symbol

$$\delta^{TT\,ij}_{kl} = \frac{1}{2}\left(\Delta_{ik}\Delta_{jl} + \Delta_{il}\Delta_{jk} - \Delta_{ij}\Delta_{kl}\right)\Delta^{-2},$$

where $\Delta_{ij} = \delta_{ij}\Delta - \partial_i\,\partial_j$. Its action is best explained using the electrodynamics analogy. When the Coulomb gauge $\nabla\cdot\mathbf{A} = 0$ is used, the vector potential $\mathbf{A}$ represents true degrees of freedom of electromagnetic field while $\Delta\Phi = -4\pi\rho$ determines immediate relation between potential Φ and charge density ρ. The vector potential satisfies wave equation $(-\partial_{tt} + \Delta)\mathbf{A} = -4\pi\,\mathbf{j}^{\mathrm{T}}$ (we assume $c = 1$), where $\mathbf{j}^{\mathrm{T}} = \mathbf{j} - (4\pi)^{-1}\nabla\partial_t\Phi$ is the so-called *transverse current* [6]. Due to charge conservation, the transverse current for localized sources can be written as $j^{\mathrm{T}}_j = \Delta_{jk}\Delta^{-1}\,j_k$, so to determine $\mathbf{j}^{\mathrm{T}}$ we no longer need to know the potential Φ, but we still need to solve a Poisson-type equation when evaluating the action of Δ^{-1} on the current density $\mathbf{j}$. Then, in the Hamiltonian approach, the transverse current appearing on the right-hand side of the wave equation for $\mathbf{A}$ arises from a projection of the variational derivative of the interaction term $-\int \mathbf{j}\cdot\mathbf{A}\;d^3x$ with respect to $\mathbf{A}$. We will see that evaluating the TT-projection operator will be the main obstacle.

In the next step, we want to eliminate the field variables and obtain the Hamiltonian function of particle variables only. Neglecting $O(G^2)$ and higher terms, we can estimate the field assuming particles' uniform motion, but this field cannot be simply substituted into the Hamiltonian (1.9), because it depends on the particle variables, and this would change the derivatives in (1.11). In the PN approximation, an approach to eliminate the gravitational field's degrees of freedom based on Routh functional was developed in [7]. Because the Routhian behaves as Hamiltonian for particles and Lagrangian for fields, its functional derivative with respect to h^{TT}_{ij} vanishes when the field equations are satisfied. Then the dependence of $h^{TT}_{ij}(\mathbf{x}_a, \mathbf{p}_a)$ appearing in the Routhian on the particle variables does not change derivatives in (1.11). Applying this method in our approximation, we effectively merge the last two parts of (1.9), changing the factor $-\frac{1}{2}$ into $-\frac{1}{4}$. This result has its analogue in classical electrodynamics too — in electrostatics, the energy in the external field $\sum_a Q_a\Phi(\mathbf{x}_a)$ acquires factor $\frac{1}{2}$ when energy of a system of charges $Q_a, a = 1, 2, ...$ is considered by putting $\Phi(\mathbf{x}) = \sum_b Q_b/|\mathbf{x} - \mathbf{x}_b|$. (The self-energy of point charges is then discarded. Note that a trickier analogy of the magnetic interaction of moving charges would be more exact.)

Substituting the solution $h^{TT}_{ij}(\mathbf{x}_a, \mathbf{p}_a)$, which describes the gravitational field of unaccelerated particles, we turn the Routhian $R[\mathbf{x}_a, \mathbf{p}_a; h^{\mathrm{TT}}_{ij}(\mathbf{x}_a, \mathbf{p}_a), \pi^{ij\;\mathrm{TT}}(\mathbf{x}_a, \mathbf{p}_a)]$ into the Hamiltonian function of particle variables $H(\mathbf{x}_a, \mathbf{p}_a)$. To obtain $h^{TT}_{ij}(\mathbf{x}_a, \mathbf{p}_a)$, we need to solve the field equations of motion in the first-order approximation

$$\Box h^{\mathrm{TT}}_{ij} \;=\; -16\pi G\;\delta^{\mathrm{TT}\,kl}_{ij}\sum_a \frac{p_{ak}p_{al}}{\overline{m}_a}\delta^{(3)}(\mathbf{x} - \mathbf{x}_a)\;. \tag{1.12}$$

Because the operations commute, we start with the Green's function of the equation $\Box f_a(\mathbf{x}) = -4\pi\delta^3(\mathbf{x} - \mathbf{x}_a)$ known as the Liénard-Wiechert potential. Its retarded solution reads [6]

$$f_a(\mathbf{x}) = \left(\frac{1}{|\mathbf{x} - \mathbf{x}_a|}\frac{1}{1 - \dot{\mathbf{x}}_a\cdot\mathbf{n}_a}\right)_{\mathrm{ret}},$$

where $\mathbf{n}_a = (\mathbf{x} - \mathbf{x}_a)/|\mathbf{x} - \mathbf{x}_a|$, but for the uniform motion of the source it is equal to the advanced solution and using $\cos\theta_a = \mathbf{n}_a\cdot\dot{\mathbf{x}}_a/|\dot{\mathbf{x}}_a|$ it can be written as

$$f_a(\mathbf{x}) = \frac{1}{|\mathbf{x} - \mathbf{x}_a|}\frac{1}{\sqrt{1 - |\dot{\mathbf{x}}_a|^2\sin^2\theta_a}}. \tag{1.13}$$

Then the position of the a-th particle $\mathbf{x}_a(t)$ is a function of the coordinate time t. The projection $\delta_{ij}^{\mathrm{TT}\,kl}$ in (1.12) involves the solution of a bi-Laplacian equation. To evaluate $\Delta^{-2} f_n(\mathbf{x})$, the usual post-Newtonian method involves expansion of f_a with respect to the velocity parameter, nevertheless, in the post-Minkowskian approximation, $\dot{\mathbf{x}}_a$ is no longer a small parameter. Because f_a was simple enough, it was possible to "experiment" with the help of computer algebra systems and find a relation

$$\Delta^2 \left(|\mathbf{x}-\mathbf{x}_a|\sqrt{1-v^2\sin^2\theta_a}\right)^3 = 3(1-v^2)^2\left[8+7v\frac{d}{dv}+v^2\frac{d^2}{dv^2}\right]\quad\left(\frac{1}{|\mathbf{x}-\mathbf{x}_a|}\frac{1}{\sqrt{1-v^2\sin^2\theta_a}}\right),$$

where $v=|\dot{\mathbf{x}}_a|$. Thus, the function $g_a \equiv \Delta^{-2} f_a$ can be found as a solution of the ordinary differential equation

$$3(1-v^2)^2\left[8+7v\frac{d}{dv}+v^2\frac{d^2}{dv^2}\right] g_a = \left(|\mathbf{x}-\mathbf{x}_a|\sqrt{1-v^2\sin^2\theta_a}\right)^3. \tag{1.14}$$

There is a unique solution regular at $v=0$ which separates into the product of a radial and angular parts

$$\Delta^{-2}\left(\frac{1}{|\mathbf{x}-\mathbf{x}_a|}\frac{1}{\sqrt{1-\dot{\mathbf{x}}_a^2\sin^2\theta_a}}\right) \;=\; |\mathbf{x}-\mathbf{x}_a|^3\; u\left(\cos\theta_a, \sqrt{1-\dot{\mathbf{x}}_a^2\sin^2\theta_a}\right)\;, \tag{1.15}$$

$$u(x,y)=\frac{1}{12}\frac{x^2-1}{1-y^2}+\frac{1}{36}\left(\frac{1-x^2}{1-y^2}\right)^2\left\{5-15yx^2+4y^3+(9y^2-15x^2)\left[x\left(\operatorname{arcth}x-\operatorname{arcth}\frac{x}{y}\right)-1\right]\right\}.$$

Despite the suspicious behavior at points $x=1$, $y=1$ and $x=y$, it is an analytic function of the subluminal particle's momentum. That can be illustrated by the PN expansion of the function

$$u(x,y)=\frac{1}{24}+\frac{1}{144}\frac{1}{m^2}\left(\mathbf{p}^2+3(\mathbf{n}\cdot\mathbf{p})^2\right)+\frac{1}{1152}\frac{1}{m^4}\left(-6(\mathbf{n}\cdot\mathbf{p})^2\mathbf{p}^2+3(\mathbf{n}\cdot\mathbf{p})^4-5\mathbf{p}^4\right)+\ldots\,. \tag{1.16}$$

Once the operation Δ^{-2} is figured out, only derivatives are needed to evaluate

$$\begin{aligned} h_{ij}^{TT}(\mathbf{x};\;\mathbf{x}_a,\mathbf{p}_a,\dot{\mathbf{x}}_a) = \frac{G}{|\mathbf{x}-\mathbf{x}_a|}\frac{1}{\overline{m}_a}\frac{1}{y(1+y)^2}\Big\{ &\left[y\mathbf{p}_a^2-(\mathbf{n}_a\cdot\mathbf{p}_a)^2(3y+2)\right]\delta_{ij} \\ &+2\left[1-\dot{\mathbf{x}}_a^2(1-2\cos^2\theta_a)\right]p_{ai}p_{aj}+\left[(2+y)\,(\mathbf{n}_a\cdot\mathbf{p}_a)^2-\left(2+3y-2\dot{\mathbf{x}}_a^2\right)\mathbf{p}_a^2\right]n_{ai}n_{aj} \\ &+2(\mathbf{n}_a\cdot\mathbf{p}_a)\left(1-\dot{\mathbf{x}}_a^2+2y\right)(n_{ai}p_{aj}+p_{ai}n_{aj})\Big\}+O(G^2), \end{aligned} \tag{1.17}$$

$$y=\sqrt{1-\dot{\mathbf{x}}_a^2\sin^2\theta_a}\;. \tag{1.18}$$

Note that the logarithms (hidden in arcth) contained in the function $u(x,y)$ disappeared. Then the interaction term $-\frac{1}{4}\sum_a \overline{m}_a{}^{-1}p_{ai}p_{aj}\,h_{ij}^{TT}$ arises solely as a function of particle variables. After self-energy is discarded and dependence on $\dot{\mathbf{x}}_a$ is removed by a canonical transformation, the

final N-body Hamiltonian in the first-order post-Minkowskian approximation is obtained,

$$H_{\rm lin} = \sum_a \overline{m}_a - \frac{1}{2}G\sum_{a,b\neq a}\frac{\overline{m}_a\overline{m}_b}{r_{ab}}\left(1+\frac{p_a^2}{\overline{m}_a^2}+\frac{p_b^2}{\overline{m}_b^2}\right)+\frac{1}{4}G\sum_{a,b\neq a}\frac{1}{r_{ab}}\left(7\,\mathbf{p}_a\cdot\mathbf{p}_b+(\mathbf{p}_a\cdot\mathbf{n}_{ab})(\mathbf{p}_b\cdot\mathbf{n}_{ab})\right)$$
$$-\frac{1}{4}G\sum_{a,b\neq a}\frac{1}{\overline{m}_a\overline{m}_b\,r_{ab}}\frac{1}{(y_{ba}+1)^2y_{ba}}\times \qquad (1.19)$$
$$\Bigg[2\Big(2(\mathbf{p}_a\cdot\mathbf{p}_b)^2(\mathbf{p}_b\cdot\mathbf{n}_{ba})^2-2(\mathbf{p}_a\cdot\mathbf{n}_{ba})(\mathbf{p}_b\cdot\mathbf{n}_{ba})(\mathbf{p}_a\cdot\mathbf{p}_b)\mathbf{p}_b^2+(\mathbf{p}_a\cdot\mathbf{n}_{ba})^2\mathbf{p}_b^4-(\mathbf{p}_a\cdot\mathbf{p}_b)^2\mathbf{p}_b^2\Big)\frac{1}{\overline{m}_b^2}$$
$$+2\left[(\mathbf{p}_a\cdot\mathbf{n}_{ba})^2(\mathbf{p}_b\cdot\mathbf{n}_{ba})^2-\mathbf{p}_a^2(\mathbf{p}_b\cdot\mathbf{n}_{ba})^2+2(\mathbf{p}_a\cdot\mathbf{n}_{ba})(\mathbf{p}_b\cdot\mathbf{n}_{ba})(\mathbf{p}_a\cdot\mathbf{p}_b)+(\mathbf{p}_a\cdot\mathbf{p}_b)^2-(\mathbf{p}_a\cdot\mathbf{n}_{ba})^2\mathbf{p}_b^2\right]$$
$$+\left[(\mathbf{p}_a\cdot\mathbf{n}_{ba})^2(\mathbf{p}_b\cdot\mathbf{n}_{ba})^2-3\mathbf{p}_a^2(\mathbf{p}_b\cdot\mathbf{n}_{ba})^2+8(\mathbf{p}_a\cdot\mathbf{n}_{ba})(\mathbf{p}_b\cdot\mathbf{n}_{ba})(\mathbf{p}_a\cdot\mathbf{p}_b)+\mathbf{p}_a^2\mathbf{p}_b^2-3(\mathbf{p}_a\cdot\mathbf{n}_{ba})^2\mathbf{p}_b^2\right]y_{ba}\Bigg],$$

where $y_{ba}=\overline{m}_b^{-1}[m_b^2+(\mathbf{n}_{ba}\cdot\mathbf{p}_b)^2]^{\frac{1}{2}}$, $r_{ab}=|\mathbf{x}_a-\mathbf{x}_b|$, and $n_{ab}=(\mathbf{x}_a-\mathbf{x}_b)/r_{ab}$.

Relation to the PN expansion of a binary system

If the Hamiltonian (1.19) is expanded in powers of $1/c^2$, one can get all PN terms linear in G. It can be compared with the PN Hamiltonian of a binary system

$$H \;=\; m_1+m_2+\frac{\mathbf{p}_1^2}{2m_1}+\frac{\mathbf{p}_2^2}{2m_2}-\frac{Gm_1m_2}{r_{12}}+H_{1PN}+H_{2PN}+H_{3PN}\;+\ldots. \qquad (1.20)$$

which has been determined up to the 3PN order in [8, 9].

The H_{1PN} and H_{2PN} implied by the Hamiltonian (1.19) are the same as those given by equations (8) and (9) in [8] once we neglect $O(G^2)$ terms given there. On the other hand, (1.19) leads to H_{3PN} which does not resemble its counterpart in [8]. Indeed, to obtain H_{3PN}, we made different canonical transformations than in [8]. Thus the particle's coordinates $\mathbf{x}'_a$ and $\mathbf{p}'_a$ used there are related to $\mathbf{x}_a$ and $\mathbf{p}_a$ here through a canonical transformation

$$\mathbf{x}'_a=\mathbf{x}_a+\{\mathbf{x}_a,\Xi\}\quad,\qquad \mathbf{p}'_a=\mathbf{p}_a+\{\mathbf{p}_a,\Xi\}\;, \qquad (1.21)$$

where the function Ξ is its generator and $\{f,g\}$ are the Poisson brackets. Since it is proportional to G, the change to 3PN term of 1PM Hamiltonian is given by the Poisson bracket of Ξ and the Newtonian kinetic term H_0 inside $\overline{m}_a$

$$H'_{3PN}(\mathbf{x}_a,\mathbf{p}_a)=H_{3PN}(\mathbf{x}_a,\mathbf{p}_a)-\{H_0,\Xi_{\rm 3PN}\}\;,\qquad H_0=\sum_a\frac{\mathbf{p}_a^2}{2m_a}\;. \qquad (1.22)$$

Then we can find that

$$\Xi_{\rm 3PN} \;=\; \frac{Gm_1m_2}{96}\left(3\frac{(\mathbf{p}_2\cdot\mathbf{n}_{12})^3(\mathbf{p}_1\cdot\mathbf{n}_{12})^2}{{m_2}^3{m_1}^2}+9\frac{\mathbf{p}_1^2(\mathbf{p}_2\cdot\mathbf{n}_{12})^2(\mathbf{p}_2\cdot\mathbf{n}_{12})}{{m_2}^2{m_1}^3}+18\frac{(\mathbf{p}_1\cdot\mathbf{p}_2)(\mathbf{p}_2\cdot\mathbf{n}_{12})^2(\mathbf{p}_1\cdot\mathbf{n}_{12})}{{m_2}^3{m_1}^2}\right.$$
$$\left.+7\frac{\mathbf{p}_2^2(\mathbf{p}_2\cdot\mathbf{n}_{12})^3}{{m_1}^3m_2^2}+3\frac{\mathbf{p}_1^2\mathbf{p}_2^2(\mathbf{p}_2\cdot\mathbf{n}_{12})}{{m_2}^3{m_1}^2}+6\frac{\mathbf{p}_1^2(\mathbf{p}_1\cdot\mathbf{p}_2)(\mathbf{p}_2\cdot\mathbf{n}_{12})}{{m_2}^2{m_1}^3}+6\frac{(\mathbf{p}_1\cdot\mathbf{p}_2)^2(\mathbf{p}_2\cdot\mathbf{n}_{12})}{{m_2}^3{m_1}^2}\right)-(1\leftrightarrow 2)\quad.$$

Recently, the respective 4PN terms were determined in [10] and as we discuss below, new post-Minkowskian results based on diagrammatic techniques appeared. The canonical transformations which would relate them to (1.19) are not yet known.

Massless particles

Even though we did assume $|v| < 1$, the Hamiltonian as well as the $h_{ij}^{\rm TT}$ in (1.17) seem to behave reasonably in the $v \to 1$ limit, so it is worth investigating this in more detail. Let us start with the test particle limit.

It is interesting that the 1PM approximation admits an unstable circular orbit of a massless particle. One can notice that it is not an obvious feature by PM expansion of the Hamiltonian for a massless test particle in the Schwarzschild spacetime with mass M. Because in "polar" canonical coordinates r, p_r, ϕ, L_z the Hamiltonian equations provide circular orbits with $p_r = 0$ if $\dot{p}_r = -\partial H/\partial r \equiv 0$, we can find the radii of the circular orbits by solving $\partial H/\partial r = 0$ after substituting $|\mathbf{p}| = L_z/r$ and $|\mathbf{x}| = r$ into the massless test particle Hamiltonian

$$H_{\rm test}(\mathbf{x}, \mathbf{p}) = \frac{1 - \frac{GM}{2|\mathbf{x}|}}{\left(1 + \frac{GM}{2|\mathbf{x}|}\right)^3} |\mathbf{p}|, \tag{1.23}$$

which can be obtained using isotropic Schwarzschild coordinates and the usual Euclidean norms for $|\mathbf{x}|$ and $|\mathbf{p}|$. Then using an expansion in G and putting $p = L_z/r$ one gets

$$H_{\rm test}(r, L_z) = \left(\frac{1}{r} - \frac{2GM}{r^2} + \frac{9G^2M^2}{4r^3} - \frac{2G^3M^3}{r^4} + \frac{25G^4M^4}{16r^5} - \frac{9G^5M^5}{8r^6} + O\left(G^6\right)\right) L_z. \tag{1.24}$$

It turns out that in the 2PM, 4PM, and 6PM approximations this function has no radial maximum and thus circular orbits do not exist in these approximations. Then, unlike in the exact solution, in 8PM, 10PM, etc., there exist stable massless particle orbits. Thus, the odd PM approximations better mimic the unstable photon orbits around black holes. The 1PM light-sphere orbital frequency is $1/(8GM)$, the true one for photons orbiting a Schwarzschild black hole has the factor $3\sqrt{3} \approx 5.2$ instead of 8. Note that in contrast to the radial coordinate of the orbit, this is a gauge-independent quantity.

In this approximation and using the center of mass system (CMS), two massless particles with $\mathbf{p}_1 = -\mathbf{p}_2 = \mathbf{p}$ can orbit each other on circular orbits (where $\mathbf{p} \cdot \mathbf{n} = 0$) forming a system with $M_{\rm ADM} = 4|\mathbf{p}|/3$. Of course, this is far beyond the validity region of the 1PM approximation, but since massless particles may be used to approximate wave packets, it is interesting to see how the theory describes the model of Wheeler's "geon".

A suitable application of the 1PM approximation is relativistic scattering where no virial theorem links the particle's momentum and radius. For massless particles, the "head-on" collision can be approximated with CMS Hamiltonian $H_{\rm 1D}(r, p_x) = 2|p_x| - 8G\,{p_x}^2/r$. In Figure 1.1 we show its phase space trajectories.

The factor y in the denominator of the metric (1.17) may become zero for null particles at planes where $(\mathbf{x} - \mathbf{x}_a)\cdot\mathbf{p}_a = 0$. We checked that the metric and implied Hamiltonian function are finite functions with discontinuous but finite first derivatives with respect to $\mathbf{x}_b$ and $\mathbf{p}_b$. It means that the particle's Hamilton equations of motion will yield discontinuous $\dot{\mathbf{x}}_b$ and $\dot{\mathbf{p}}_b$ when the particle passes through planes where $\mathbf{n}_{ba}\cdot\mathbf{p}_a = 0$. Similar singular features are typical for the gravitational field of a source moving at the speed of light, which is known to be accompanied by an impulsive wave localized on a null plane (associated with a null coordinate $u = 0$) following the source [11]. Depending upon the chosen coordinates, the metric may contain a discontinuity of the first derivative in a form of a "kink" $\sim u + |u|$ or, surprisingly, even an impulse in the form of a δ-function $\delta(u)$. The Hamiltonian (1.19) leads to a behavior similar to the former

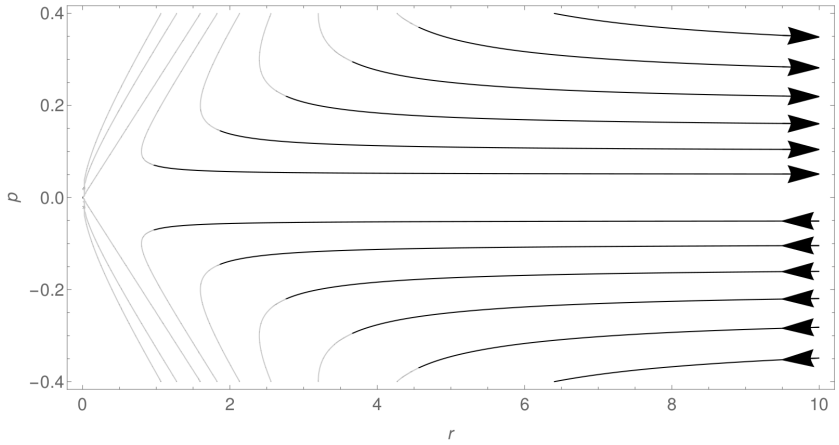

Figure 1.1: The phase space trajectories of the head-on/radial motion of two massless particles in 1PM approximation in CMS. Due to homogeneity of the problem, arbitrary (but the same) length units are used on the axes. The thin lines indicate region where system becomes very compact ($r < 12|p|$) and the approximation is not valid. If massless particles model compact massless field wave packets, growth of $|p|$ during the approach is due to a blueshift.

type of impulsive waves accompanying massless components of the many-body system — in the linear order their effects simply superimpose.

There is an interesting feature of the 1PM N-body Hamiltonian and the fact that this approximation allows to describe motion of massless particles — some of the particles can be considered (test) photons passing through gravitationally interacting many-body systems and they can be used to describe gravitational lensing in such situations.

Recent developments in PM approximation of general relativity

An obvious application of PM approximation is the relativistic scattering of gravitating relativistic particles. In [P1] we show that the scattering angle implied by (1.19) agrees with the results obtained by other methods. In recent years, new approaches to PM approximation have emerged, reaching very recently the 4PM order. One approach, the effective field theory formalism, models compact objects as gravitationally interacting point-like massive particles and has been applied in the post-Minkowskian (PM) expansion scattering trajectories [12]. Another approach uses a massive scalar field for a similar purpose [13]. This has also enabled to compute the gravitational waves produced by such scattering encounters [14]. These results are based on the methods of quantum field theory and path integrals, e.g., they require summation of $\sim 10^2 - 10^5$ diagrams, so they are rather complicated already at 1PM approximation. Although they now clearly surpass the results presented here, hopefully, the relative simplicity of the derivation of (1.19) still makes this result useful.

1.1.2 Hamiltonian for a spinning test particles in Kerr spacetime

With the ever growing precision of various measurements available in modern astronomy, there is also a growing interest in the impact of rotation on various astrophysical phenomena involving general relativity. An example of such an effect is a 1974 prediction of the disappearance [15, 16] of a binary pulsar PSR 1913 + 16 due to pulsar precession. Now, the spins of merging black

holes are estimated from the detected gravitational waves.

In Hamiltonian approach, let us mention two important impulses — a great progress in Hamiltonian description of orbiting spinning bodies followed the work [17], and Hamiltonian description of a spinning test particle in curved spacetime was given in [18]. In this section, a brief description of extension of the latter work will be given. Even though the equations of motion of a spinning test body in curved spacetime date back to 1937 [19], their Hamiltonian version describing the motion of a spinning particle around a rotating black hole came only after 60 years [18]. The main obstacle turned out to be the fact that the particle's canonical momentum and spin are hard to find so that the right Poisson-Dirac bracket relations hold in the curved spacetime.

One of the astrophysical processes, where the spin of the body plays an important role is so-called extreme-mass-ratio inspiral, a situation where, e.g., a stellar-mass spinning black hole orbits around a much (even 10^8-times) heavier supermassive black hole. The orbiting black hole radiates gravitational waves broadcasting a very detailed message about the gravitational field in which it moves and also about its own spin. This process is assumed to happen in galactic centers and the generated gravitational waves should be registered by the planned space GW observatory LISA.

Introduction

While point particles are in general relativity moving along geodesics $Dp^\mu/d\tau \equiv U^\kappa \nabla_\kappa p^\mu = 0$, where the four-velocity $U^\mu = dx^\mu/d\tau$ and momentum $p^\mu = mU^\mu$ are simply related, the Mathisson-Papapetrou-Dixon equations governing the motion of spinning particles are more complicated. Using a modern transcription of the results [19, 20, 21] they read

$$\frac{D}{d\tau}\, p^\mu = -\frac{1}{2}\, R^\mu{}_{\nu\kappa\lambda}(x^\rho) U^\nu S^{\kappa\lambda}, \tag{1.25}$$

$$\frac{D}{d\tau}\, S^{\mu\nu} = p^\mu\, U^\nu - U^\mu\, p^\nu. \tag{1.26}$$

The point particle is still assumed to follow the worldline $x^\mu(\tau)$ with tangent 4-vector $U^\mu = dx^\mu/d\tau$ in a curved spacetime with Riemann tensor $R^\mu{}_{\nu\kappa\lambda}$, but it also carries the spin tensor $S^{\mu\nu}$. The relation between momentum and 4-velocity is no longer as simple. Because the center of mass of a spinning extended body depends on the choice of the inertial system, it is hard to assign to it an unambiguous worldline. In addition, the system of 10 equations (1.25), (1.26) is underdetermined and various so-called spin supplementary conditions (SSCs) have been suggested to reduce the number of independent variables from 13 to 10 (see, e.g., [22, 23]). Once SSC is chosen, the relation between U^μ and p^μ is also given.

In the Hamiltonian formulation of the problem x^μ, p^μ and $S^{\mu\nu}$ are reduced to canonical variables x^i, P_i and S^I (spin vector), $i, j, I = 1, 2, 3$ which have to satisfy numerous relations for Poisson-Dirac brackets. In [18] a generalized Newton-Wigner SSC is found to lead to canonical variables satisfying these relations neglecting higher-order (spin-squared) terms. Then the

Hamilton equations have a usual form (ϵ_{IJK} is Levi-Civita symbol)

$$\frac{dx^i}{dt} = \frac{\partial H}{P_i}, \tag{1.27}$$

$$\frac{dP_i}{dt} = -\frac{\partial H}{x^i}, \tag{1.28}$$

$$\frac{dS_I}{dt} = \epsilon_{IJK}\frac{\partial H}{S_J}S^K. \tag{1.29}$$

The Hamiltonian of the spinning particle in the curved background is then $H = H_{\rm NS} + H_{\rm S} + O(S^2)$, where the nonspinning part is

$$H_{\rm NS} = N^i P_i + N\sqrt{m^2 + \gamma^{ij}P_iP_j}. \tag{1.30}$$

The lapse N, shift N_i, and spatial metric γ_{ij} are defined by the line element (1.2). The canonical momenta P_i are different from "kinetic" momenta p_i — they are shifted proportionally to the spin of the particle in way analogous to canonical momenta of a charged particles with "shift" proportional to their charge. Main complication comes from the fact that the canonical spin vector

$$S_I = \frac{1}{2}\epsilon_{IJK}\,\tilde{e}^J_\mu\,\tilde{e}^K_\nu\,S^{\mu\nu}, \tag{1.31}$$

is defined using tetrad field $\tilde{e}^0_\mu$, $\tilde{e}^I_\mu$, which provides set of orthogonal directions at each point of the spacetime. Derivatives of this tetrad fields then enter the formula for P_i and the spinning part of the Hamiltonian $H_{\rm S}$ needs even more auxiliary fields (see [18] or less detailed exposition in [P2]).

Thus, to obtain Hamiltonian of a spinning test particle in Kerr spacetime, a tetrad field has to be chosen and then it is necessary to evaluate all the steps proposed in [18]. A natural choice followed in [18] was the tetrad aligned with the Boyer-Linquist coordinates. These coordinates are known to have many appealing properties and allowed to evaluate the full, still rather complicated, Hamiltonian. Main motivation for the new research was the fact that this tetrad is similar to the one based on the usual spherical coordinates and thus even a noninteracting particle moving very far away from the black hole has a nontrivial spin evolution, because the almost constant spin tensor is projected onto the tetrad field which is changing along the particle's trajectory. In [P2] we have shown that this leads to an undesired violation of angular momentum conservation for Hamiltonian description of the orbital motion around a spherical Schwarzschild black hole which was traced back to the neglected $O(S^2)$ terms in Hamiltonian [18]. As a cure we have found that under the same conditions a zero-angular-momentum-observer (ZAMO) tetrad derived from Kerr-Schild coordinates conserves angular momentum. In a final step, a new tetrad was devised which enabled to analytically evaluate all necessary steps and arrive at quite concise version of the spinning test particle Hamiltonian in Kerr metric. This part will be described below in more detail.

Hamiltonian of a spinning test particle in Kerr spacetime

We use Kerr-Schild coordinates x, y, z, t in which the Kerr black hole metric with mass M, angular momentum J and rotation parameter $a = J/M$ resembles the Minkowski metric in Cartesian coordinate system,

$$ds^2 = g_{\mu\nu}dx^\mu\,dx^\nu = (\eta_{\mu\nu} + f\;l_\mu\;l_\nu)\,dx^\mu dx^\nu, \tag{1.32}$$

where $f(x,y,z;M,a)$ is an axisymmetric function and $l_\mu(x,y,z;a)$ is a special null vector field, $g^{\mu\nu}l_\mu l_\nu = 0$, which is also null with respect to the flat Minkowski metric, $\eta^{\mu\nu}l_\mu l_\nu = 0$, $\eta_{\mu\nu} = \eta^{\mu\nu} = \mathrm{diag}(-1,1,1,1)$. This feature simplifies many calculations. (For detailed expressions for f and l_μ see [P2].) We found that Kerr-Schild coordinates enable to construct the appropriately normalized orthonormal tetrad field

$$e_\mu{}^A = \eta^{AB}\left(\eta_{\mu B} + \frac{f}{2}l_\mu l_B\right), \qquad g^{\mu\nu}e_\mu{}^A e_\nu{}^B = \eta^{AB}, \qquad \mu,\nu,A,B = 0,1,2,3, \tag{1.33}$$

without the need to include additional square root factors, otherwise typical for normalized vector fields. Because the derivatives of these tetrad components enter the Hamiltonian, this simplification led to a shorter analytic form of the Hamiltonian $H = H_{\rm NS} + H_{\rm SO} + H_{\rm SS}$ (partitioned into non-spinning (NS), spin-orbital (SO) and spin-spin (SS) parts)

$$H_{NS} = \alpha^2 f\ l_i P_i + \alpha\sqrt{m^2 + P_iP_i - f\alpha^2(l_iP_i)^2}\ , \tag{1.34}$$

$$H_{SO} = \alpha f\frac{Mm - 2\widetilde{m}(M - fr)}{2M\ \overline{m}\ \omega_T}\ \frac{r\ \epsilon^{ijK}l_i p_j S^K}{r^2 + a^2 l_z^2}\ , \tag{1.35}$$

and

$$H_{SS} = -\frac{af}{4\,\omega_T\ M\overline{m}\ (a^2l_z^2 + r^2)} \times \Bigg\{\Big[4\,f l_z\,\widetilde{m}\,((\overline{m} - \alpha f\widetilde{m})r + \alpha\widetilde{m}M) - 2M\,l_z\left(\overline{m}m + \alpha m^2\right)$$
$$+ 2\,\alpha\,[(M + 2\,r)mfl_z + (3M - 2fr)P_z]\,\widetilde{m}\Big]S^i l_i + 2\,\alpha\,(m + \widetilde{m})\left[Ml_z\ S^iP_i - \widetilde{m}\,(2\,fr - 3M)\,S^3\right]$$
$$- 2\,\frac{al_z\,\widetilde{m}}{r^2}\left(3\,Mr - a^2 f{l_z}^2 - 3\,fr^2\right)\Big[\alpha(S^1P_y - S^2P_x) - (\alpha m + \overline{m} - \alpha f\widetilde{m})\,(S^1l_y - S^2l_x)\Big]\Bigg\}\ .$$

where

$$\alpha = \frac{1}{\sqrt{1+f}},\quad \overline{m} = \sqrt{m^2 + P_iP_i - f\alpha^2(l_iP_i)^2},\quad \widetilde{m} = \alpha\overline{m} - \alpha^2 P_i l^i,\quad \omega_T = -m - \frac{\overline{m}}{\alpha} + \frac{f}{2}\widetilde{m}.$$

The current application is limited to studies of the chaos introduced in the completely integrable motion of the point particle in the Kerr geometry [24] when the particle acquires a spin. It has to be determined if there are other implications of the change of the tetrad from the Boyer-Lindquist one (called *curvature aligned* in [25]) to the Kerr-Schild tetrad (1.33), e.g., when terms containing the second power of the particle's spin are considered.

1.2 Dragging effects of gravitational waves

When the first Newton's law is understood as a postulate that there exists some inertial system where free uninteracting bodies remain at rest or in uniform motion, it sidesteps the question with respect to 'what' this system stays at rest or in uniform motion. Mach's argument that it must be all those far-away stars reflected the simple cosmology of his day. Nevertheless, it is a nice and influential idea even now when the local inertial systems are known to exist in the form of the spacetime metric of the expanding universe.

Mach's idea, its role in the birth of general relativity, as well as the actual influence of the surrounding matter (e.g, in the form of slowly rotating shells) on the inertial frame in its center are all thoroughly studied [26, 27]. Such rotation can be distinguished from the gauge effect because it can be observed — if the central frame is equipped with a gyroscope, its axis will rotate with respect to stars on the sky of the central observer, see Fig 1.2.

Einstein theory predicts the existence of gravitational waves (GWs) and that they can carry energy or angular momentum. This has been observed in binary pulsar systems and verified by the detection of gravitational waves by LIGO. However, if gravitational waves can carry energy and angular momentum, can they also exert Machian influence?

I had the opportunity to join J. Bičák, D. Lynden-Bell, and J. Katz in their investigation of the dragging effects of the angular momentum of gravitational waves. New results extend their previous study of gravitational waves with the translational symmetry along z-axis [28] and thus also with an infinite energy of the gravitational waves. In the following, I will focus on the part of the problem I contributed to the papers [P3] and [P4].

Introduction

To study the dragging effects of the angular momentum of gravitational waves, a suitable wave packet is the one forming a shell surrounding the gyroscope in the center of a purely vacuum, regular, and asymptotically flat spacetime. For its description, it is convenient to use the black hole perturbation theory [29]. In this approach, instead of two polarizations, the gravitational waves are described in spherical coordinates by even- and odd-parity perturbations with angular numbers $l = 2, 3, ...$, $m = -l, ...l$. We consider perturbations of a flat Minkowski spacetime in

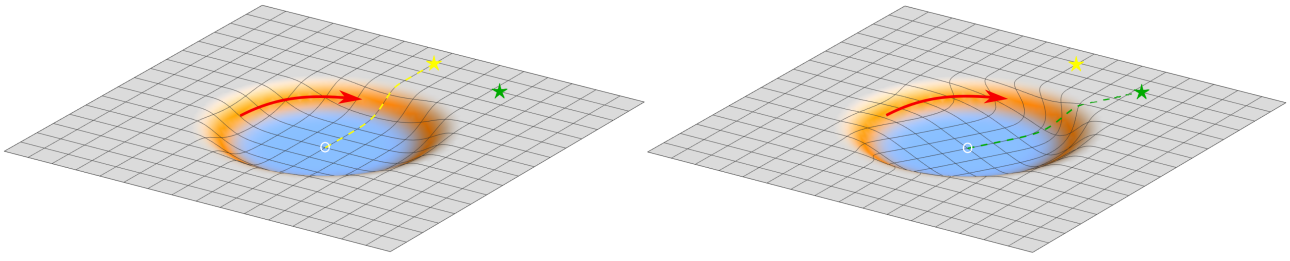

Figure 1.2: An illustration of the dragging effect of a rotating shell (orange) on a space (gray). A symmetric shell leaves the spacetime inside (blue) flat, its "gravity well" is indicated by vertical displacement. An observer in the center of a rotating massive spherical shell sees that axis of a gyroscope rotates with respect to distant stars (so it first points to the yellow and later to the green star). Direct influence of the shell on the light ray (dashed) and timing effects are neglected in this illustration.

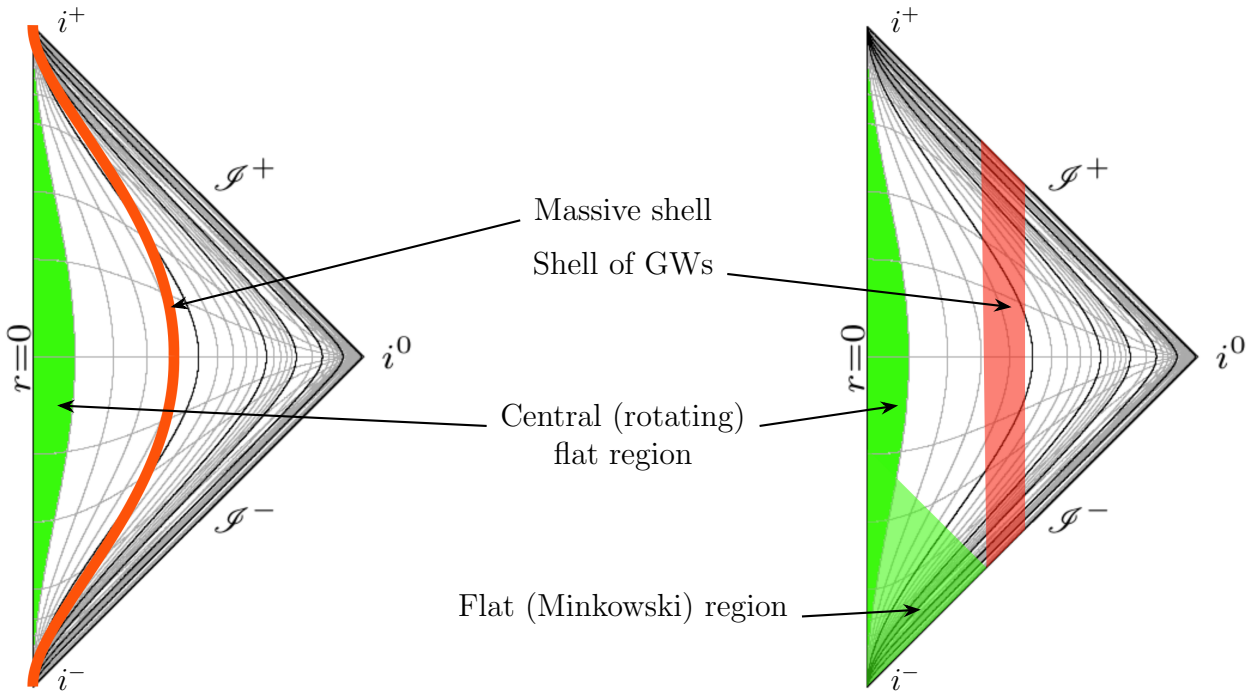

Figure 1.3: Compactified conformal diagrams of an approximately Minkowski spacetime with rotating shell made of massive particles (left) and gravitational waves (right). In these diagrams the curves ending at the spatial infinity i^0 are hypersurfaces of constant Minkowski time t and the curves connecting the past infinity i^- with the future infinity i^+ are worldlines of constant spatial Minkowski coordinates. The conformal character of the plot means that radial null worldlines (of ingoing and outgoing photons) are 45° lines. The radiation character of gravitational waves causes that the considered GW shell of finite width emerges from the past null infinity $\mathscr{I}^-$ so unlike for the massive shell, the spacetime contains also flat region near past infinity i^-.

the form

$$g_{\mu\nu} = \eta_{\mu\nu} + h^{(1)}_{\mu\nu} + h^{(2)}_{\mu\nu} + ... \tag{1.36}$$

where $\eta_{\mu\nu} = \mathrm{diag}(-1, 1, r^2, r^2 \sin^2\theta)$ is a flat Minkowski metric in spherical coordinates t, r, θ, φ, and $h^{(1)}_{\mu\nu}$ and $h^{(2)}_{\mu\nu}$ are the first and second-order perturbations of the flat spacetime. The Einstein equations $G_{\mu\nu}[g] = 0$ can be then decomposed according to the order of perturbation. The gravitational waves enter as the first-order solution to the linearized Einstein equation

$$G^{(1)}_{\mu\nu}[h^{(1)}] = 0, \tag{1.37}$$

where $G^{(n)}_{\mu\nu}[h]$ is a shortcut for terms of n-th order in h contained in the expansion of the Einstein tensor $G_{\mu\nu}$. The gravitational effects of these waves appear in the second-order perturbation to the metric which satisfies

$$G^{(1)}_{\mu\nu}[h^{(2)}] = -G^{(2)}_{\mu\nu}[h^{(1)}, h^{(1)}]. \tag{1.38}$$

Here $G^{(2)}_{\mu\nu}[h^{(1)}, h^{(1)}]$ contains terms of $G_{\mu\nu}$ quadratic in first-order perturbation amplitude. The right-hand side contains the same linear operator as (1.37) but applied to ${}^{(2)}h_{\mu\nu}$. A simple fact, that the metric field of gravitational waves can be changed by a first-order gauge transformation

$$h'^{(1)}_{\mu\nu} = h^{(1)}_{\mu\nu} + \xi^{(1)}_{\mu,\nu} + \xi^{(1)}_{\nu,\mu} \tag{1.39}$$

has important consequences. Such change modifies $G^{(2)}_{\mu\nu}[h^{(1)}, h^{(1)}]$ in (1.38) which thus cannot be understood as well-defined stress-energy tensor of gravitational waves unless the high-frequency limit is considered [30]. For the studied shape of the GW shell, this will be the limit of high angular parameter l. Moreover, we will assume that $\xi^{(1)\mu}$ are restricted to the same spacetime region as gravitational wave perturbations $h^{(1)}_{\mu\nu}$ so the first-order perturbations leave the flat Minkowski spacetime in the shell center untouched and terms quadratic in $h'^{(1)}$ do not contaminate $h^{(2)}$ in the center. We will also discuss that a gauge-independent total rotation can be derived from the gauge- and slice-dependent quantities.

Dragging inside a gravitational-wave shell

We use the usual decomposition of the odd-parity perturbations for both $h^{(1)}_{\mu\nu}$ and $h^{(2)}_{\mu\nu}$

$$h^{(i)}_{\mu\nu} = \sum_{lm} \begin{pmatrix} 0 & 0 & -h^{(i)}_{0lm}(t,r)\frac{1}{\sin\theta}\partial_\varphi Y_{lm} & h^{(i)}_{0lm}(t,r)\sin\theta\partial_\theta Y_{lm} \\ 0 & 0 & -h^{(i)}_{1lm}(t,r)\frac{1}{\sin\theta}\partial_\varphi Y_{lm} & h^{(i)}_{1lm}(t,r)\sin\theta\partial_\theta Y_{lm} \\ ... & ... & -\frac{1}{2}h^{(i)}_{2lm}(t,r)\frac{1}{\sin\theta}X_{lm} & \frac{1}{2}h^{(i)}_{2lm}(t,r)\sin\theta W_{lm} \\ ... & ... & ... & \frac{1}{2}h^{(i)}_{2lm}(t,r)\sin\theta X_{lm} \end{pmatrix}_{\mu\nu}, \tag{1.40}$$

where $X_{lm} = 2\partial_\varphi\left(\partial_\theta - \cot\theta\right)Y_{lm}$ and $W_{lm} = \left(\partial^2_\theta - \cot\theta\partial_\theta - \sin^{-2}\theta\partial^2_\varphi\right)Y_{lm}$ [29, 31].

Field equations for perturbations are usually written in the frequency domain components (see, e.g., [32]), but to describe shell-forming pulses of waves we explicitly retain the time dependence of the perturbations. Evolution equations in the time domain can be found in [33] for the case of Reissner-Nordström black hole background, which can be simplified to Minkowski

case by setting the mass and charge of the black hole to zero. Assuming now the Regge-Wheeler gauge $h^{(1)}_{2lm} = 0$ the first-order odd-parity perturbations of the Minkowski spacetime satisfying (1.37) turn out to be equivalent to a simple wave equation

$$\Box\psi = 0. \tag{1.41}$$

Its solution ψ then determines following nonzero components of $h^{(1)}_{\mu\nu}$:

$$h^{(1)}_{t\theta} = \frac{1}{\sin\theta}\frac{\partial^2}{\partial r\,\partial\varphi}(r^2\psi), \qquad h^{(1)}_{t\varphi} = -\sin\theta\frac{\partial^2}{\partial r\,\partial\theta}(r^2\psi), \tag{1.42}$$

$$h^{(1)}_{r\theta} = \frac{1}{\sin\theta}\frac{\partial^2}{\partial t\,\partial\varphi}(r^2\psi), \qquad h^{(1)}_{r\varphi} = -\sin\theta\frac{\partial^2}{\partial t\,\partial\theta}(r^2\psi). \tag{1.43}$$

The fact that ψ may be composed from several spherical harmonic components and does not necessarily contain a complex factor $e^{im\varphi}$ is convenient. Because for second-order perturbations we must consider only the real part of $h^{(1)}_{\mu\nu}$ we will later directly use a real function ψ solving (1.41).

The form of perturbations (1.40) is a particular form of a general decomposition into tensor harmonics. It is an analogy to the decomposition of a simple scalar function $f(\theta,\varphi)$ on a sphere into the sequence f_{lm} such that $f = \sum_{l,m} f_{lm}Y_{lm}(\theta,\varphi)$. Here Y_{lm} are scalar spherical harmonics, while in Eq. (1.40) appear also the vector and tensor harmonics [34] made of the first and second order angular derivatives of Y_{lm}.

When the frame rotation velocity ω_0 along the $z-$axis is considered for a flat Minkowski spacetime in spherical coordinates

$$ds^2 = -dt^2 + dr^2 + r^2\,d\theta^2 + r^2\,\sin^2\theta\,\left(d\varphi - \omega_0\,dt\right)^2, \tag{1.44}$$

the term linear in ω_0 appears in $g_{t\varphi} = -\omega_0\,r^2\sin^2\theta$. Thus, among the second-order perturbations $h^{(2)}_{\mu\nu}$ expressed in the form (1.40) we are interested in $l = 1, m = 0$ component

$$h^{(2)}_{t\varphi} = -\sqrt{\frac{3}{4\pi}}h^{(2)}_0(t,r)\sin^2\theta = -\omega_0\,r^2\sin^2\theta, \tag{1.45}$$

where the square root factor originates from $Y_{10}(\theta,\varphi)$ in (1.40). As is usual in the decomposition into mutually orthogonal spherical harmonics, also for the tensor harmonics can be each partial wave component obtained independently as a scalar product with the respective harmonic basis function. Thus, to get the equation for ω_0 the set of equations (1.38) has to be multiplied by a particular tensor spherical harmonics and integrated over the sphere $r = \text{const}$. Retaining the second-order perturbations on the left-hand side and the quadratic expression made from the first-order perturbations on the right-hand side, the relevant equation reads

$$\frac{1}{2}\left[h^{(2)\prime\prime}_0 - \frac{l(l+1)}{r^2}h^{(2)}_0 - \dot{h}^{(2)\prime}_1 - \frac{2}{r}\dot{h}^{(2)}_1\right] = \frac{1}{l(l+1)}\int_0^{2\pi}\int_0^{\pi} R^{(2)}_{t\varphi}[h^{(1)},h^{(1)}]\partial_\theta Y_{l0}\;d\theta\;d\varphi. \tag{1.46}$$

Using a global change of coordinate $\varphi \to \varphi + \delta\varphi^{(2)}(t,r)$ we can set

$$h^{(2)}_1 = 0 \quad \text{i.e.} \quad h^{(2)}_{r\varphi} = 0. \tag{1.47}$$

Then near the center we have the Minkowski metric in spherical coordinates with the dominating perturbation corresponding to slow rigid rotating of the central frame with angular velocity

$\omega_0(t)$. Fixing the gauge condition (1.47), $h^{(2)}_{1\,l=1,m=0} = 0$, prohibits any radial dependence of an additional coordinate transform $\varphi \to \varphi + \delta\varphi^{(2)}(t,r)$ and the angle φ in the center and thus also the central frame rotation ω_0 is unambiguously determined with respect to spatial infinity i^0. There are no other $l = 1, m = 0$ odd gauge modes, W_{lm} in (1.40) vanishes for $l \leq 1$.

With this gauge condition the Eq. (1.46) for $l = 1, m = 0$ becomes the second-order radial ordinary differential equation which can be analytically solved and (1.45) then yields

$$\omega_0 = \frac{1}{4\pi} \iiint R^{(2)}_{t\varphi}[h^{(1)}, h^{(1)}] \, \frac{\sin\theta}{r} dr \, d\theta \, d\varphi. \tag{1.48}$$

To build a detailed model of gravitational waves in the form of a rotating wave packet, a particular exact solution of flat-space wave equation

$$\psi = \frac{A_{lm} P^m_l(\cos\theta) \; \tilde{r}^l}{\left[(1+\tilde{r}^2-\tilde{t}^2)^2 + 4\tilde{t}^2\right]^{(l+1)/2}} \cos\left[m\varphi - \lambda(t,r)\right], \tag{1.49}$$

where

$$\tilde{r} = \frac{r}{a}\,, \quad \tilde{t} = \frac{t}{a} \quad \text{and} \quad \lambda(t,r) = (l+1)\arctan\frac{2\tilde{t}}{1+\tilde{r}^2-\tilde{t}^2}, \tag{1.50}$$

has been obtained by the Fourier transform of a simpler one given in the frequency domain [P3]. This function describes a spherical shell of waves converging from infinity, bouncing at radius $r \approx a$ and then dispersing again. This was inspired by the waves studied by Bičák, Lynden-Bell, and Katz [28] who generalized the axisymmetric pulses of Weber and Wheeler [35]. Number of wave crests in θ and φ directions is determined by usual partial wave indices l, m. Its amplitude, here denoted A_{lm}, then determines the strength of gravitational waves. The particular form (1.49), i.e. the separated form with polynomial dependence on $\cos\theta$, harmonic in φ and with a tractable dependence on the radial coordinate r, allows us to evaluate analytically all integrals in (1.48).

There is no obvious way to demonstrate how spacetime is deformed by gravitational waves at each point. Instead, we will take advantage of relation (1.43) and discuss features of the function ψ. The waves (1.49) form a shell of radiation bouncing at the origin with the thickness of the shell decreasing with growing l. This is demonstrated in Fig. 1.4. The function vanishes at the origin as r^l so for high enough values of l, near the origin it is smaller than the considered second-order metric perturbations. Similarly, it goes as $1/r^{l+2}$ as $r \to \infty$. This effectively makes the support of the function ψ limited to an interval centered around the wave packet off-center null worldline with $r \approx \sqrt{a^2+t^2}$ (see Fig. 1.5 for explanation). The radial half-width of the wave packet decreases with l as $\Delta r_{1/2} \doteq \sqrt{8\ln 2}\; a\; l^{-1/2}$. This enables us to describe analytically an arbitrarily thin shell.

In [P3] we describe the necessary steps which are needed to compute the integral (1.48). Because the Ricci tensor contains quadratic terms built from second-, third- and fourth-order derivatives of the function ψ we needed help from the computer algebra system MAPLE. Even then we had to extend its capabilities, among others, by rules for integration of functions given in Appendices A and C of [P3]. The final closed-form formula for $\omega_0(t)$ is given by a rather complicated formula (7.10) there. Here let us discuss its approximate version which assumes $l \gg 1$:

$$\omega_0(t) \doteq \frac{\omega_0^{\max}}{\left(1+\frac{t^2}{a^2}\right)^{3/2}}. \tag{1.51}$$

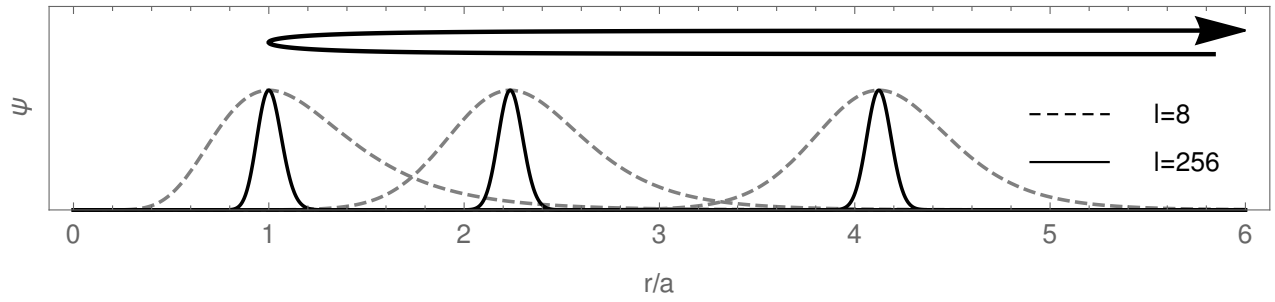

Figure 1.4: The radial envelope of the function ψ at selected times $t = -4a, -2a, 0, +2a, +4a$. At each time it determines the width of the spherical shell wave packet. The temporal dependence of the shell radius is indicated at the top, the shell thickness is controlled by the parameter l.

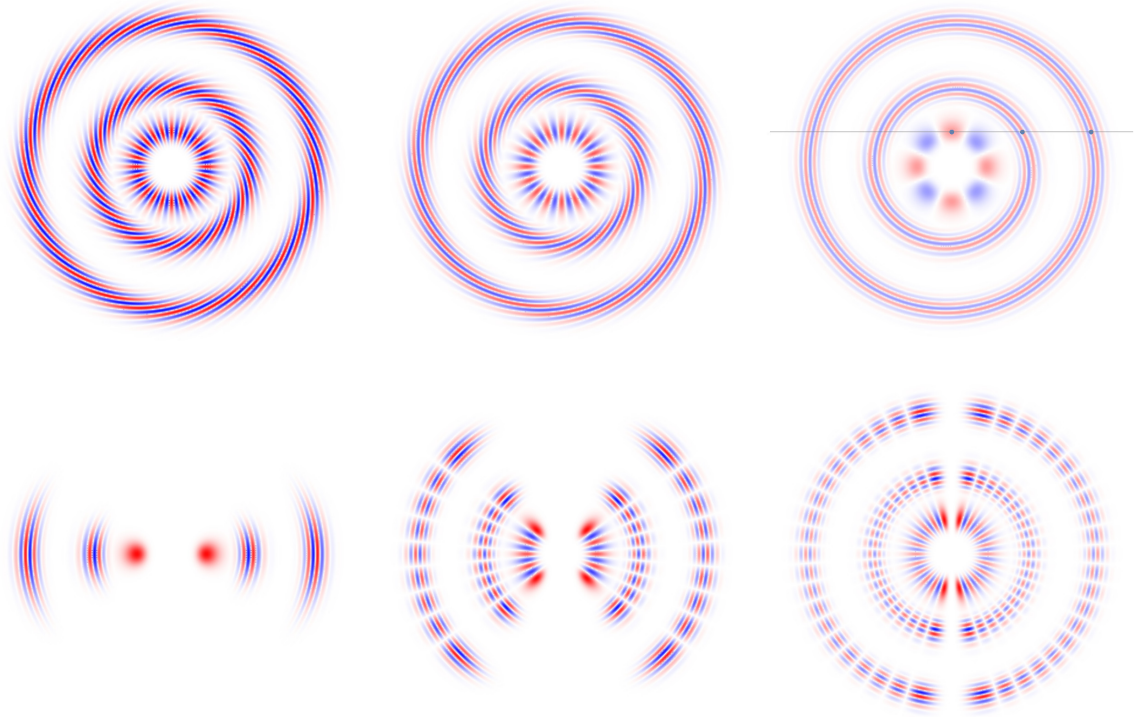

$l = 24, m = 24$ $l = 24, m = 16$ $l = 24, m = 4$

Figure 1.5: Snapshots of the function ψ in the equatorial plane $\theta = \pi/2$ (top) and in the meridional plane $\varphi = 0, \pi$ (bottom) at three distinct times $t = 0, 2a, 4a$. The well-known behavior of spherical harmonics $Y_{lm} \sim \sin^{|m|}\theta$ means that for higher m first order perturbations vanish not only near the center where we study frame dragging but also along the z axis. The top right plot also illustrates position of a null particle with $\mathbf{r} = a\hat{\mathbf{y}} + t\hat{\mathbf{x}}$ at given times to illustrate the localization of the wave at radii $r \approx \sqrt{a^2 + t^2}$. (We denote Cartesian unit vectors $\hat{\mathbf{x}}, \hat{\mathbf{y}}$, red/blue color indicates positive/negative ψ.)

In the same limit, we show in [P4] that the frame dragging is determined by the angular momentum of the gravitational wave L_z and that the long exact formula can be approximated by $\omega_0^{\max} \doteq 2L_z/a^3$. The angular momentum of the linearized gravitational waves is defined using the effective stress energy tensor

$$L_z = -\int T^{\text{eff}}_{t\varphi}\, d^3x, \qquad T^{\text{eff}}_{t\varphi} = \frac{1}{8\pi} R^{(2)}_{t\varphi}[h^{(1)}, h^{(1)}]. \tag{1.52}$$

We can see that (1.48) and (1.52) differ by a factor r^3 inside the integral. This explains why the approximate relation(1.51) holds: because for $l \gg 1$ the function ψ is localized around a thin shell with radius $r(t) \doteq \sqrt{a^2 + t^2}$, the factor r^3 can be put in front of the integral.

Such results may be surprising, because they may seem acausal. To see this, let us discuss the situation from the spacetime perspective in Fig. 1.6. In this figure there is emphasized a region where due to causality, one cannot know that a converging shell of waves is approaching. Nevertheless, the time dependence (1.51) gives nonzero rotation ω_0 in this region. While it may seem strange, this is consistent with the role of ω_0. As we mentioned under the Eq. (1.46) the angular velocity ω_0 is defined with respect to the spatial infinity i^0 because at each time t the gauge condition $h^{(2)}_{1\,l=1,m=0} = 0$ fixes orientation of the central inertial frame because it prohibits any radial dependence of coordinate transform $\varphi \to \varphi + \delta\varphi^{(2)}(t, r)$. Thus only $\delta\varphi^{(2)}(t)$ is allowed and we see that fixing this at infinity means we first made limit $r \to \infty$ and then consider finite t. Thus, the limiting procedure defining the gauge and ω_0 selects the $t = \text{const.}$ hypersurfaces in Fig. 1.6 ending at the spatial infinity i^0.

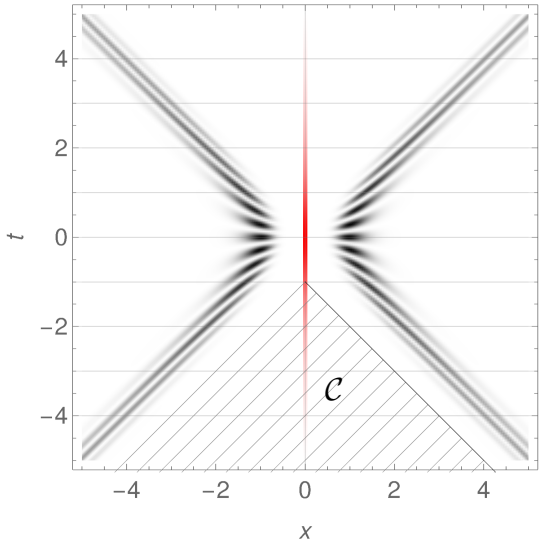

Figure 1.6: The $x - t$ plane of a spacetime diagram showing the central region surrounded by a bouncing shell of rotating gravitational waves (gray). Because the shell has finite width and it is made from null radiation there is a spacetime region $\mathcal{C}$ (dashed) where the information about incoming GW pulse is not available. Horizontal lines represent hypersurfaces $t = \text{const.}$ which play role in the definition of the angular velocity of the central frame rotation ω_0 indicated by the color intensity of the central worldline — the second-order perturbation determining ω_0 are constrained by the gauge condition applied on $t = \text{const.}$ hypersurfaces. Unlike the dashed region $\mathcal{C}$, all $t = \text{const.}$ hypersurfaces cross the GW shell. This is the reason, we get nonzero ω_0 also inside $\mathcal{C}$.

As we argued, the first-order perturbation do not enter the central region $r \ll a$ and for second order perturbations in sufficiently small neighborhood of the origin we can also neglect $h^{(2)}_{\mu\nu\, lm}$ with $l > 1$. Thus, there exists a flat worldtube with Minkowskian metric connecting the past and future infinities, i^- and i^+. Since the studied spacetime is asymptotically flat, there also exists well-defined patch of Minkowski spacetime far from the centre. These two patches meet at $i^\pm$ but do not contain spacetime region of nonvanishing ψ.

In both flat patches there exists well-defined nonrotating inertial frame, e.g., by stars far from the center and by the gyroscopes in the center. In Fig. 1.7 we illustrate that the rotation of the central inertial frame may be understood as a spacetime version of the well-known demonstration of the parallel transport on the sphere, where the gyroscope axis is the vector transported either along the central geodesic or staying far away from the center and from the influence of the gravitational wave. When their axes are aligned in i^-, they will mismatch at i^+.

Perturbations of ingoing null rays by GW shell

A telescope fixed to a set of gyroscopes would observe a real change of the celestial coordinates of stars. Apart from the second order dragging effect, there will be a deflection of the light ray in the gravitational wave. It can be computed by the integration of the perturbative version of the geodesic equation. In [P3] we showed that the variations $\delta\theta$ and $\delta\varphi$ of the celestial positions as seen by the gyroscope-stabilized telescope at the center have for gravitational waves (1.43) appealing analytic form

$$\frac{\delta\varphi}{\Delta\varphi} + i\frac{\delta\theta}{\Delta\theta} = i^{l-1}\frac{e^{im\varphi_\star}}{\left(1 + i\frac{T}{a}\right)^{l+2}}, \tag{1.53}$$

where $\Delta\theta = m\psi_{\max}(\theta_\star)/(4l\sin\theta_\star)$ and $\Delta\varphi = \psi_{\max}(\theta_\star)P'^m_l(\cos\theta_\star)/[4lP^m_l(\cos\theta_\star)]$ are the amplitudes of the apparent motion expressed using the dimensionless amplitude scale of the gravitational waves $\psi_{\max}(\theta) = \psi(r = a, t = 0, \theta, \varphi = 0)$ which depends only on direction θ. The motion of the star's image due to bending of the light ray in the field of the gravitational wave is explained in Fig. 1.8. Given the obvious θ-dependence of the wave as is shown in Fig. 1.5, both amplitudes $\Delta\theta, \Delta\varphi$ vary with the star celestial latitude $\theta_\star$ and so does the eccentricity of the apparent star trajectory on the celestial sphere which is shown in Fig. 1.9.

In [P3] we did not investigate second-order perturbations of the incoming star light rays. However, we know that at both $t \to \pm\infty$, i.e. i^- and i^+ second-order metric perturbation vanish and the total central frame rotation

$$\Delta\varphi_0 = \int_{-\infty}^{\infty} \omega_0(t)\, dt \tag{1.54}$$

translates into the changed position of stars on the central observer's sky. In Fig. 1.9(d) we sketch this effect. In Fig. 1.7 we illustrate $\Delta\varphi_0$ as an obvious implication of the spacetime curvature due to rotating gravitational waves. Thus, although the immediate value of ω_0 involves instantaneous effects, its integral (1.54) representing the total rotation of the central gyroscope is well-defined observable quantity. In the approximation $l \gg 1$ we then obtain $\Delta\varphi_0 \doteq 2a\omega_0^{\max} \doteq 4L_z/a^2$. Such a simple relation is not available for dragging by a massive rotating shell, because its dynamics is not as unambiguous as that of gravitational radiation.

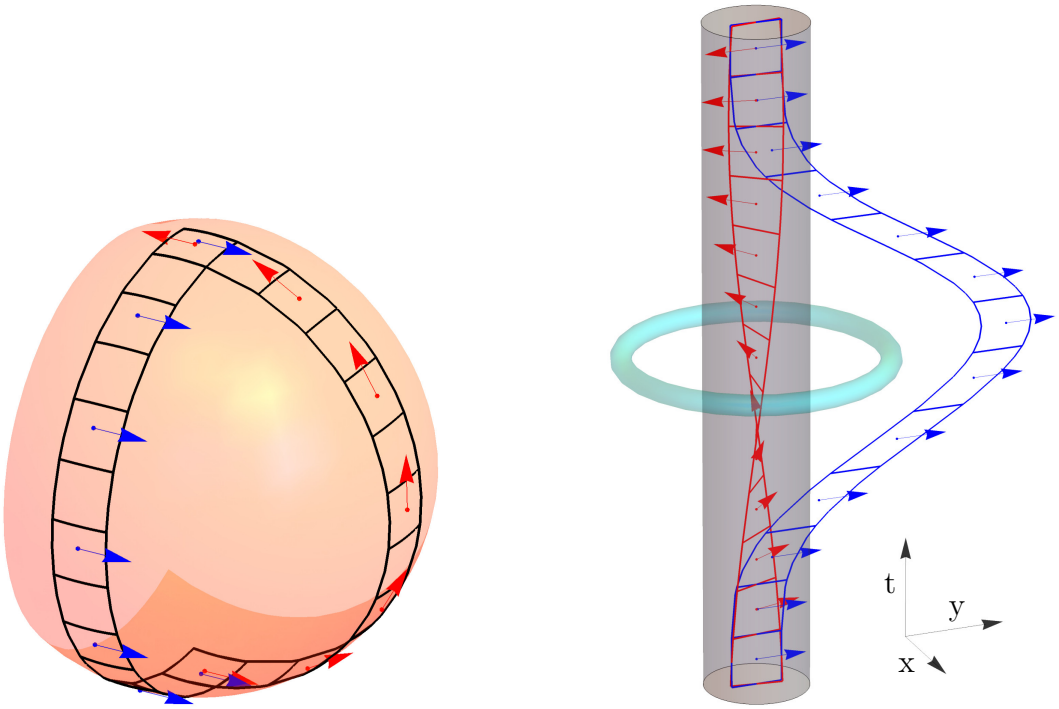

Figure 1.7: *Left:* The fundamental dependence of parallel transport on the chosen path is usually demonstrated on a sphere surface naturally embedded in three-dimensional flat Euclidean space. Here we use neighborhoods of two meridians as an example of two approximately flat patches which yield mismatch when vector from the south pole is extended into both patches. *Right:* In our spacetime with rotating gravitational waves we have also two approximately flat patches. The spacetime is asymptotically flat which is in the figure symbolized by blue "ladder" with arrows indicating "fixed" direction of a gyroscope. Because the gravitational waves do not reach the center, there is also approximately flat region near the center. Its worldtube is depicted as a gray cylinder. The gravitational waves are shown in the moment they are strongest ($t = 0$) as a blue torus encircling the central observer. The rotation of the central inertial frame (and gyroscopes there) is illustrated by the twist of the red spacetime-coordinate "ladder" and gyroscope orientation. The mismatch of gyroscope directions at the top demonstrates meaning of Eq. (1.54) as implication of a particular form of spacetime curvature accompanying the rotating gravitational wave.

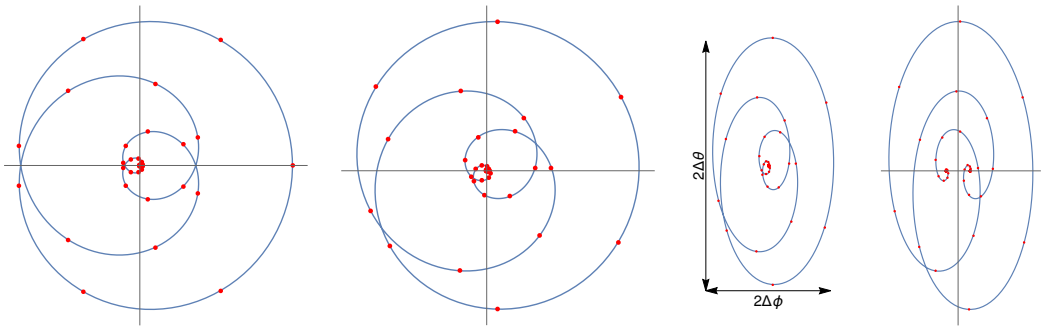

(a) (b) (c) (d)

Figure 1.8: Trajectory on the celestial sphere of the apparent star position (1.53) influenced by gravitational wave (1.43) with $l = 18$ as it is observed by the central observer. The image arises as a complex map $(1 + iz)^{-2-l}$ of the real axis (a). Speed of this apparent motion is demonstrated by red points at $t/a = j/20$, $j \in \mathbb{Z}$. According to (1.53) it is then rotated by the phase factor $e^{im\varphi_\star}$ (b) and finally scaled by $\Delta\varphi$ and $\Delta\theta$ (c). The second order effects will rotate the inner frame with respect to stars while the apparent star position would wiggle due to first-order effects. A combination of these effect is in an exaggerated form illustrated on the panel (d).

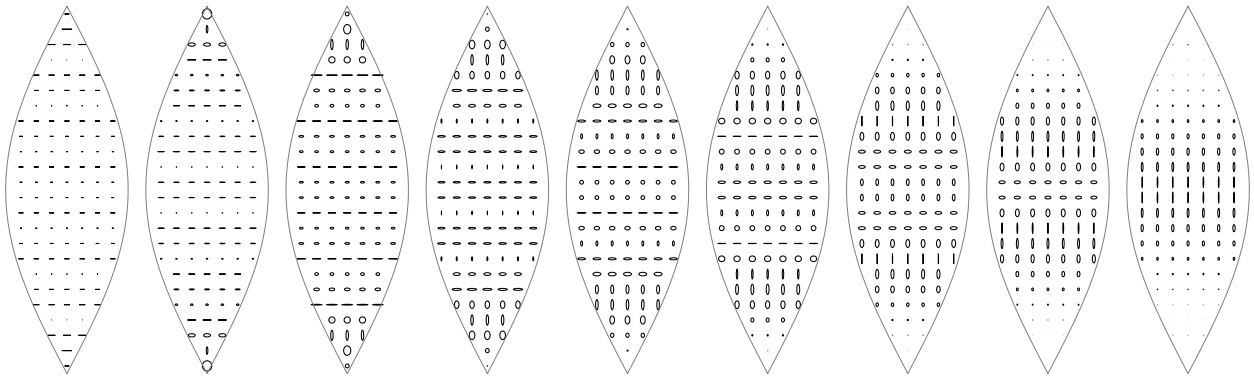

$m = 0$ $m = 1$ $m = 2$ $m = 3$ $m = 4$ $m = 5$ $m = 6$ $m = 7$ $m = 8$

Figure 1.9: The celestial trajectories from Fig. 1.8 would look in the telescope like spirals from Fig 1.8(c) bounded by ellipses with semi-axes $\Delta\varphi \sin\theta_\star$ and $\Delta\theta$ which depend on star's celestial coordinates θ_*, φ_*. Such ellipses are shown here for $l = 8$ and various m as they would appear on a patch of sky delimited by two meridians.

1.3 Gravitational collapse of gravitational waves

Introduction

The concept of a super-extremely compact star from which even light cannot escape dates back to Michel a Laplace [36]. Astronomy of the 20th century showed that such object may arise by gravitational collapse of dying stars and general relativity brought understanding that such dead star, called black hole, is a stable object made from nothing but empty curved spacetime and contains a spacetime singularity surrounded by one-directional membrane, *event horizon* — the sphere defining a black hole.

When gravitational collapse into a black hole is discussed, usually the first picture one has on mind is the 1939 spherically symmetric model of collapsing dust by Oppenheimer and Snyder. [37]. It describes ball made of a pressureless dust, which collapses without any opposition toward the center. At some moment the light emanating outward from the ball surface finds itself falling toward the center too. The last photons which do not converge toward the center, but also do not fly away, form the event horizon. The importance of this model also emanates from the hand-drawn spacetime diagram by R. Penrose [38]. For a simplified and less artistic plot of dust and light worldlines during gravitational collapse, see Fig. 1.10.

When real matter is involved, many aspects of the simple model of the gravitational collapse remain, but a significant complication arises from well known tendency of fluids to form shocks — let us mention the magnificent phenomenon of supernova. A significant change of the process may arise if rotation of collapsing matter plays role. Not only this is important from the astrophysical point of view, but rotation brings in some new theoretical phenomena.

For a theoretician, the collapsing matter can easily be replaced by some field. There are many possibilities, but with Einstein's general relativity, we do not need additional fields then the gravitation itself. As we have seen, the gravitational waves carry energy and if enough of them is put into a small volume... Here comes the problem: energy of gravitational waves is non-local quantity. Thus for gravitational waves we do not have an unambiguous counterpart of the energy density in the Oppenheimer-Snyder collapse model. Instead, we can probe the geometry of any time slice and check if it contains (apparent) horizon. Then there is a black hole and the horizon area is used to get its (slice-dependent) mass. Also, the gravitational waves cannot be spherically symmetric (in 3+1 dimensions) and thus their gravitational collapse differs significantly from the gravitational collapse. This is another aspect showing for gravitational waves we cannot rely on our experience with usual collapsing matter.

One of the long-term puzzles of general relativity is the cosmic censorship conjecture [39]. While it has been shown that singularities are inevitable result of the gravitational collapse, in typical scenario the singularity lies inside the event horizon and cannot be seen from outside (see also Fig. 1.10). So called *critical collapse* is one of (non-generic and thus harmless) possibilities to create "naked singularity" in a numerical experiment. In many situations, but typically when massless radiating field is involved, we can take, a large amount of energy, but fine-tune its compactness so that most of the energy escapes toward the infinity, before the remaining field forms a tiny black hole. The limit, when its mass is zero was found to contain naked singularity, but another, very unexpected behavior was observed for spherically symmetric collapse of massless scalar field near this limit by Choptuik in 1993 [40]. This was so surprising that many people started checking and analyzing critical collapse of other fields. It turned out that gravitational waves, which cannot be spherically symmetric, are really hard to fine-tune and even today we are still limited by available computer power. Some

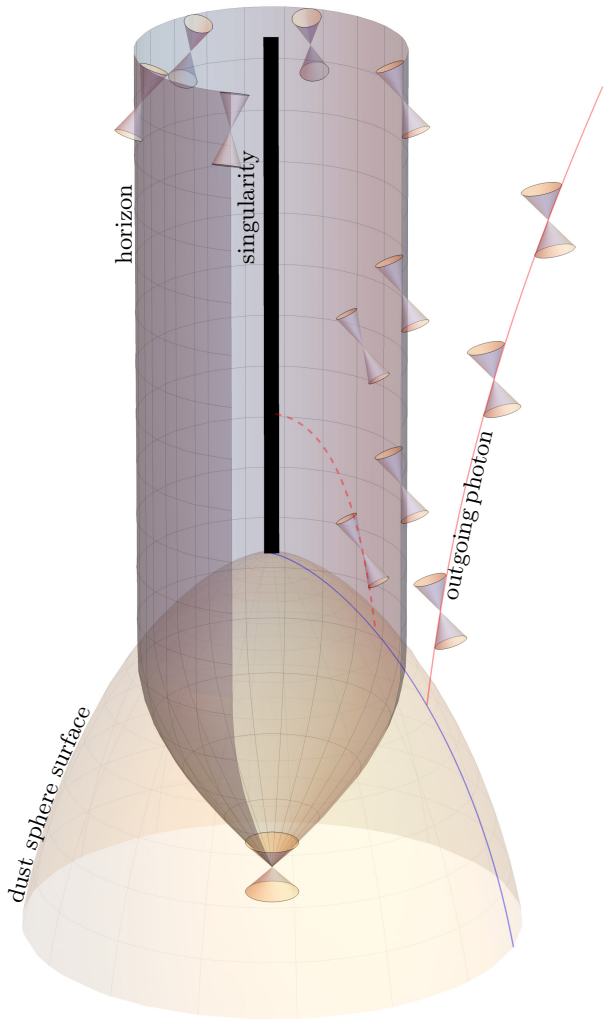

Figure 1.10: The spacetime diagram of a black hole forming in a spherically symmetric collapse of dust. Light cones indicating spacetime direction of photon worldlines are shown. While the special relativity explains that worldlines of massive particles lie everywhere inside a light cone, the general relativity has specified how these light cones are tilted by matter. Unsurprisingly, without inner pressure a dust sphere collapses due to its gravity. The spacetime diagram shows, that when the dust sphere becomes compact enough, the light cones are so tilted, that the outward-moving particles of light stay "at place" forming the black hole horizon. Photon (red solid line) which left the same place at the surface (blue line) earlier can escape, but light which leaves the surface later (dashed red line) due to the orientation of light cones inside the black hole ends up in the singularity (black thick line). The diagram also illustrates so-called cosmic censorship. The singularity is formed only after it is covered by horizon and cannot be seen from the outside. Unlike in this special case of homogeneous ball of dust, for generic spherically symmetric collapse the singularity may be formed "before" the surface reaches it (see Fig. 5.1 in [38]).

new insights into critical collapse of the gravitational waves are the main result presented in this part of the thesis. It is based on the results of simulations performed by A. Khirnov, who during his Ph.D. mastered all the necessary knowledge from the field of general relativity, numerical mathematics, and computer science making this progress possible. As an example let me mention an implementation of the novel spacetime slicing which required to develop a multigrid method (solving curved-space elliptic equation) cooperating with existing mesh refinement infrastructure of the CACTUS system for GR simulations [41].

Einstein equations in 3+1 formulation

The prediction is the key aspect in physics. The mathematical description of problems it tackles thus often relies on the ordinary differential equations and their initial conditions or on the evolutional partial differential equations for which so-called Cauchy problem defines well-posed deterministic problem. In both situations equations can be both second-order (e.g. the second Newton law) and first order in time (Hamiltonian dynamics).

We have seen that gravitational field in the Hamiltonian approach is described on hypersurfaces $t = \text{const.}$ by their inner 3-metric and the associated momenta. We will use here the standard notation of numerical relativity (see e.g. [42] where the 3+1 reduction of the Einstein equations is explained in detail), Greek indices $\mu, \nu, ... = 0, 1, 2, 3$ for spacetime tensors and Latin indices $i, j, ... = 1, 2, 3$ for spatial ones. We have to distinguish curvature tensors of the hypersurface $t = \text{const.}$, e.g. R_{ij}, and that of the 4-dimensional spacetime, ${}^{(4)}R_{\mu\nu}$. To match the notation of numerical relativity, instead of N and N^i defined in (1.2) from now on we use α for lapse and β^i for shift, but to make the equations simpler we will assume the shift function to vanish everywhere. Then the metric of the spacetime we study has form

$$ds^2 = -\alpha^2 dt^2 + \gamma_{ij} dx^i dx^j. \tag{1.55}$$

Instead of the time derivatives of γ_{ij} it is useful to introduce the geometrically defined extrinsic curvature tensor K_{ij} of the $t = \text{const.}$ with its trace denoted $K = \gamma^{ij} K_{ij}$. (Here we again use the usual approach and conventions of numerical relativity, instead of π^{ij} of Section 1.1.) The covariant derivative compatible with γ_{ij} is denoted D_i (and for $g_{\mu\nu}$ we have ∇_μ).

Than the principal pair of equations implied by the vacuum Einstein equations ${}^{(4)}G_{\mu\nu} = 0$ is in 3+1 approach written as

$$\partial_t \gamma_{ij} = -2\alpha K_{ij}, \tag{1.56}$$

$$\partial_t K_{ij} = -\mathrm{D}_i \mathrm{D}_j \alpha + \alpha \left(R_{ij} + K K_{ij} - 2 K_{ik} K^k_j \right). \tag{1.57}$$

The Einstein equations also imply the Hamilton and momentum constraints

$$R + K^2 - K^{ij} K^{ij} = 0, \tag{1.58}$$

$$\mathrm{D}_j K^{ij} - \mathrm{D}^i K = 0. \tag{1.59}$$

We will discuss later that an additional equation determining evolution of the lapse α must be supplied. Also, some additional improvements of the evolution equations are necessary to obtain well behaved (strongly hyperbolic [42, 43]) system of evolution partial differential equations (PDEs). We used existing implementation of so-called BSSN equations [44, 45] implemented as McLachlan code [46] in the Einstein Toolkit — a community computational infrastructure for relativistic astrophysics [41]. Let us also for simplicity ignore the boundary

near the spatial infinity. Then we have an initial value problem where we supply the initial data $\gamma_{ij}(x^k, t = 0)$, $K_{ij}(x^k, t = 0)$ satisfying the constraints (1.58) and (1.59) and then we use the Einstein equations to the find the outcome of the gravitational collapse.

Initial data with strong gravitational waves

Apart from diffeomorphisms, in axisymmetric and reflection-symmetric vacuum spacetime there remains one free real-valued function determining gravitational waves. In the linearized regime it describes gravitational waves with the '+'-polarization in the equatorial plane and vanishing along the symmetry axis. Such linearized problem is similar to shell-like waves we considered as source of dragging, where all metric functions (1.43) were determined by single function ψ satisfying wave equation (1.41), but this time we have the even-parity waves with no φ-dependence. In the strong-field regime the Einstein equations represent a complicated nonlinear PDE system where the single dynamical degree of freedom of the axisymmetric vacuum gravitational field is hidden in four non-zero components γ_{ij} and unlike in the linearized regime it cannot be isolated into some 'master equation'. Thus, the complete axisymmetric tensor fields γ_{ij} and K_{ij} must be specified as initial data and then evolved. (An alternative, characteristic formulation of the Einstein equations (see [47]) enables easier insight into the structure of equations, but it assumes special coordinates based on radial null geodesics, which are not available when light bending makes these geodesics cross each other.)

A Cauchy problem for a simple flat-space wave equation $\Box u = 0$ has two particular initial data categories: The initial field amplitude family $u(t = 0, x^i) = f(x^i), u_t(t = 0, x^i) = 0$ and the initial field momentum family $u(t = 0, x^i) = 0, u_t(t = 0, x^i) = g(x^i)$. We will study similar two basic initial data categories for axisymmetric gravitational waves. The so-called seed function, a counterpart to $f(x^i)$ and $g(x^i)$ above, will initially either force a deformation of the initial slice metric or the initial extrinsic curvature.

We will consider several one-parameter families of initial data which always approach a flat spacetime near infinity. The parameter then determines the amount of gravitational waves concentrated near the center. The first family has $K_{ij}(t = 0) = 0$ (i.e., it describes time-symmetric spacetime invariant with respect to the change $t \to -t$) and $\gamma_{ij}(t = 0)$ can be written in spherical coordinates r, θ, φ as

$$\gamma_{ij}(t = 0)\, dx^i\, dx^j = \psi^4 \left[e^{2q}(dr^2 + r^2 d\theta^2) + r^2 \sin^2\theta d\varphi^2 \right]. \tag{1.60}$$

There, the seed function $q(r, \theta)$ determines an axisymmetric deformation of the initial slide. The conformal factor ψ is found by solving the Hamilton constraint (1.58), the momentum constraint is trivially satisfied. To compare our results with the previous results which are reviewed in [48] we will use the seed function

$$q(x^i) = A\, \frac{r^2}{\sigma^2} e^{-\frac{r^2}{\sigma^2}} \sin^2\theta. \tag{1.61}$$

Here A is the parameter determining strength of the deformation and σ is a length scale of the problem. Because there is no other scale present, all fields scale trivially when σ in the initial data (1.61) is changed.

In an asymptotic region near the spacelike infinity I^0 we can measure the ADM mass (1.8). Thus, we know how much energy in the form of the gravitational waves the initial slice contains. For Brill initial data, this mass can be expressed in several ways using volume or surface integrals. Checking that all such alternatives agree is a simple test of the numerical precision

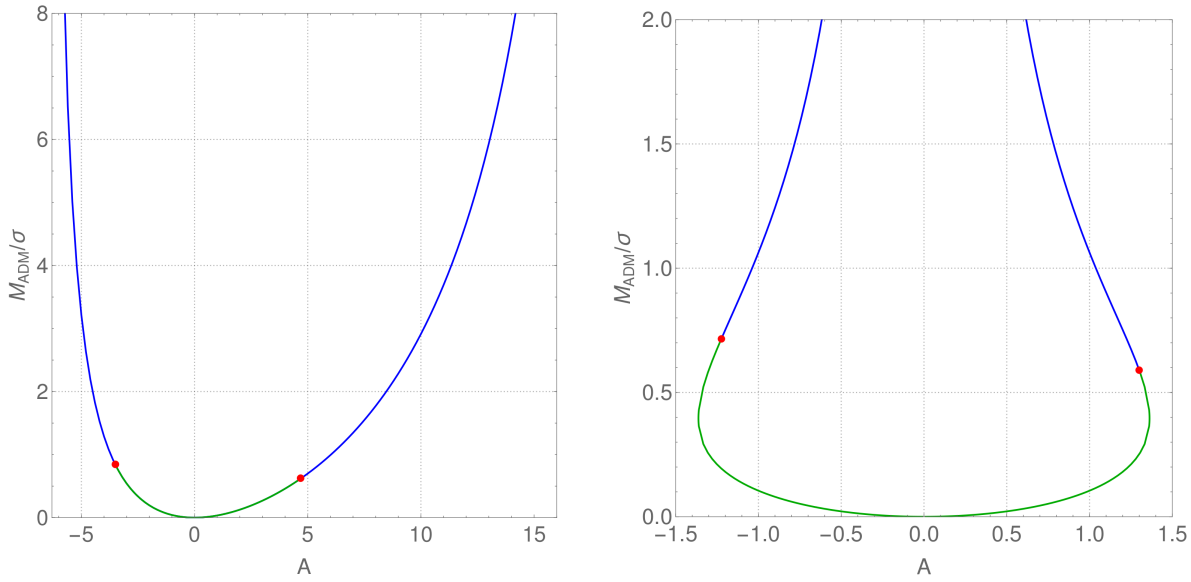

Figure 1.11: The dependence of the ADM mass of the spacetime with gravitational waves on the amplitude A of the Brill (left) and TA (right) initial data. Points on both curves indicate critical values of the parameter A. For smaller $|A|$ (green curve) the gravitational disperse and leave behind an empty space. Stronger initial data lead to black holes.

reached, a test which was not trivial in the beginnings of numerical relativity as is mentioned in the pioneering 1977 study by Eppley [49]. One of these formulas, $2\pi M_{\rm ADM} = \int \psi^{-2}|\nabla\psi|^2 d^3x$, was also important theoretically as an illustration by Brill that even strong gravitational waves have positive energy [50] and we will call this family Brill initial data.

For the complementary (initial field momentum) initial data, the seed function is put into components of K_{ij} while $\gamma_{ij} = \psi^4\delta_{ij}$ is chosen to be conformally flat. Instead of the decomposition (1.7) we tried to follow the previous work on critical GW collapse [51] and consider as a seed function the component $K^r_\theta(x^i, t=0)$. For axisymmetric initial data, the constraints then reduce to three coupled equations for ψ, $K^r{}_r$ and $K^\varphi{}_\varphi$. After several experiments with various profiles of K^r_θ we selected

$$K^r_\theta(x^i, t=0) = A\frac{r^2}{\sigma^3}(\sigma - r)e^{-\frac{r^2}{\sigma^2}}\sin 2\theta. \tag{1.62}$$

We call this family of initial data 'time-asymmetric' (TA) because non-zero K_{ij} implies that the evolution in the future direction has a different outcome than the evolution in the past.

Both initial data families lead to a flat Minkowski spacetime for $A = 0$. For small $|A|$ the energy of gravitational waves which appears as the ADM mass of the initial slice grows $\sim A^2$, nevertheless, in general, the dependence of $M_{\rm ADM}$ on the parameter A must be found numerically. We illustrate it in Fig. 1.11. For the Brill initial data, the asymmetry $A \leftrightarrow -A$ appears and $M_{\rm ADM}$ diverges at finite values of A (see [49] for explanation). The surprising shape of the dependence $M_{\rm ADM}(A)$ for TA initial data appears due to the nonlinearity of the coupled system of constraint equations (1.58),(1.59). We can get a rough algebraic relation between $M_{\rm ADM}$ and A replacing the Hamilton constraint PDE with a model algebraic equation. Using the Laplacian Δ in flat coordinates, the Hamilton constraint for TA initial data reads $8\Delta\psi = -\psi^5 K^{ij}K_{ij}$. Then estimating that $K^{ij}K_{ij} \sim A^2$ and that the conformal factor mass dependence is roughly $\psi - 1 \sim M$ and $\Delta\psi \sim -M$ we can reduce the Hamilton constraint into

the relation $A^2 \sim M/(M+4\mu)^5$, where μ is the mass for which $|A| = A_{\max}$. Plot of such curve is quite similar to the real $M_{\rm ADM}(A)$ dependence in Fig. 1.11.

The fact that for TA initial data the nonlinear constraint PDEs have two solutions for $0 < |A| < A_{\max}$ and none for higher $|A|$ complicates the process of initial data construction. We use an iterative Newton-Raphson method to solve the set of nonlinear coefficient equations generated by the pseudospectral method [52]. For small $|A|$ the iteration can be started with flat space initial data. For larger $|A|$, the solutions obtained for smaller $|A|$ can be used as an iteration starting point. Such process ends at $A = A_{\max}$. To get solutions in the upper branch we extrapolated the dependence of the spectral expansion coefficients and obtained an approximate solution for which the iteration converges to the solution on the upper branch.

Slicing conditions

The Einstein equations are invariant with respect to the change of coordinates, which in the 3+1 approach means that both shift and lapse can be chosen arbitrarily. Nevertheless, not all choices are acceptable, because with black holes some worldlines have only a limited time span and we might be forced to exclude black-hole interiors from simulations by the introduction of inner boundaries. The breakthrough in numerical relativity based on the *moving puncture* method [53] confirmed that the standard receipt for a time-coordinate choice, so-called $1 + \log$ lapse [54] in the form

$$\partial_t \alpha = -2\alpha K, \tag{1.63}$$

behaves well not only in the linearized regime and for black holes born from an approximately spherical gravitational collapse of matter or field but also during their mergers. (These situations nevertheless require $\beta^i \neq 0$ which we for simplicity ignore in (1.63).)

Surprisingly, the gravitational collapse of strong gravitational waves, even when they are weak enough to eventually dissipate, deforms the spacetime so that the simulations using (1.63) break down [55]. We studied this behavior in [P5] and shown that the hypersurfaces $t = \text{const.}$ develop a nonsmooth normal field. Of course, the process of solving of the Einstein equations requires smooth coordinates and there exists a well-known coordinate choice which prevents similar pathologies. The so-called *maximal slicing* $K = 0$ due to its extremal nature (such a slice has maximal volume for a given boundary) cannot develop sharp features [42], because these are in contradiction with the extremality of the slice. Recall that $K = K_i{}^i$ is determined by evolution equation (1.57) from which it is clear that $\partial_t K = 0$ may be guaranteed by an appropriate choice of α. This requires to solve an elliptic PDE which is computationally much more expensive then (1.63).

In [P5] we suggest a method of computing the lapse α approximately and show that it does not spoil the well-posedness of the PDE system, does not lead to constraint violations, and that it allows to evolve spacetime with collapsing gravitational waves. This approach led to an elliptic equation for a gauge source function W appearing as an additional term on the right-hand side of Eq. (1.63), $\partial_t \alpha = -2\alpha K + W$. It is similar to the direct application of a maximal slicing which leads to an elliptic equation for α, but with our approach W does not have to solve that equation exactly as long as the time-slice remains a smooth hypersurface which significantly improves effectiveness. On the other hand, the inexact determination of the lapse function for the maximal slicing approach leads directly to constraint violations. Because the evolution equation for the lapse function (1.63) is part of a system of PDEs, its modification may spoil the well-posedness of the whole system. This is checked by the analysis of the hyperbolicity of the linearized system, which shows that W can be neglected because it contains no terms linear

in the amplitude of perturbations. This modification thus does preserve the well-posedness of any evolution system using $1 + \log$ slicing. This *quasi-maximal slicing* (QMS) then allowed us in [P6] to reach a resolution necessary to study the critical collapse of gravitational waves.

Invariants in axisymmetric GW collapse

The diffeomorphism invariance of general relativity complicates the interpretation of tensor fields appearing as simulation results, only spacetime scalar quantities are immune. In vacuum gravitational collapse, it is thus common to use the Kretschmann curvature invariant $I_K \equiv R^{\kappa\lambda\mu\nu}R_{\kappa\lambda\mu\nu}$, because simpler curvature tensor invariants vanish. Usually it is the only invariant quantity studied, because similar scalars involving covariant derivatives of the Riemann tensor are hard to evaluate numerically with the necessary precision.

The main reason we assume axial symmetry in our study of the gravitational collapse of gravitational waves is that this symmetry significantly reduces the computational complexity. Nevertheless, we also utilize this symmetry to provide additional invariant scalars which help us to understand how the collapse unfolds. From the axial symmetry Killing vector field ξ^μ we get the circumferential radius $\rho \equiv (\xi^\mu\xi_\mu)^{1/2}$ and square of its gradient $\eta \equiv (\nabla^\mu\rho)\nabla_\mu\rho$. Note that in strong gravitational fields $\nabla_\mu\rho$ can become time-like or can point toward the axis. This also excludes ρ as a global coordinate.

Both ρ and η are trivial along the symmetry axis. We thus define the additional scalar quantity $\zeta \equiv (1 - \eta)/\rho^2$, where we must take an appropriate limit at the symmetry axis $\rho = 0$. Then it turns out that at the axis ζ determines the only non-vanishing projection of the Weyl tensor $\Psi_2 = \zeta/2$ onto an axis-aligned null tetrad (for the definition of Newman-Penrose curvature scalars see, e.g., [56]). It also means that at the symmetry axis the Kretschmann scalar $I_K = 12\zeta^2$. Because of this relation, another scalar quantity $I_\zeta \equiv (I_K - 12\zeta^2)/\rho^2$ indicates departure of the curvature from the spherically symmetric Schwarzschild solution for which $I_\zeta \equiv 0$.

We illustrate how various invariants look for the considered initial data in Figures 1.12 and 1.13.

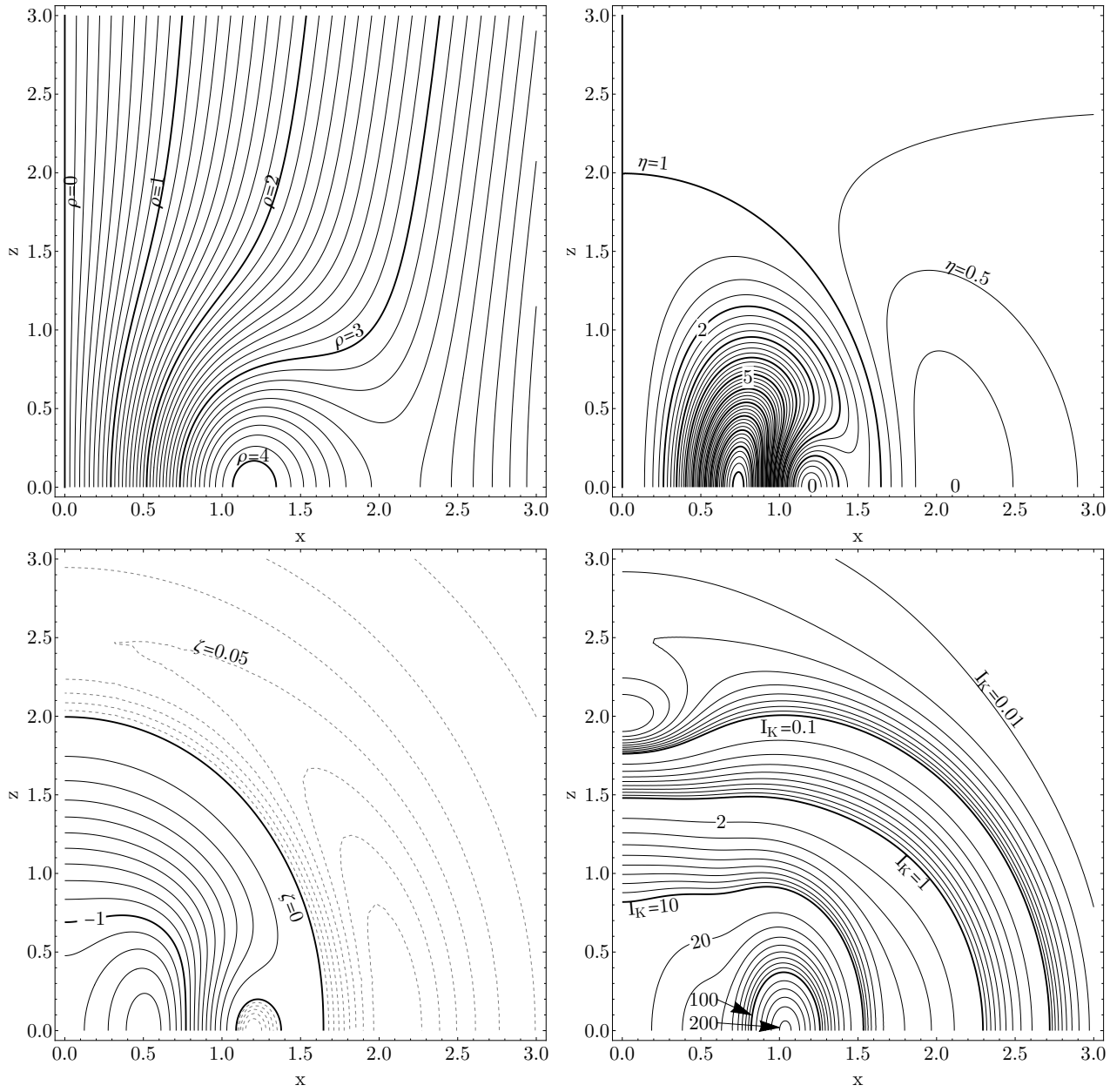

Figure 1.12: Geometry of the initial slice with Brill initial data illustrated by the values of spacetime invariants. The Brill initial data with $\sigma = 1, A = -3.6$ have $K_{ij} = 0$ and the GW 'seed' appears in γ_{ij}. This can be seen in the top plots — the initial γ_{ij} makes ρ non-monotonous and $\eta = 0$ where $\partial_i \rho$ vanishes. At larger coordinate radii the spacetime resembles the Schwarzschild geometry and ζ and I_K become approximately spherically symmetric.

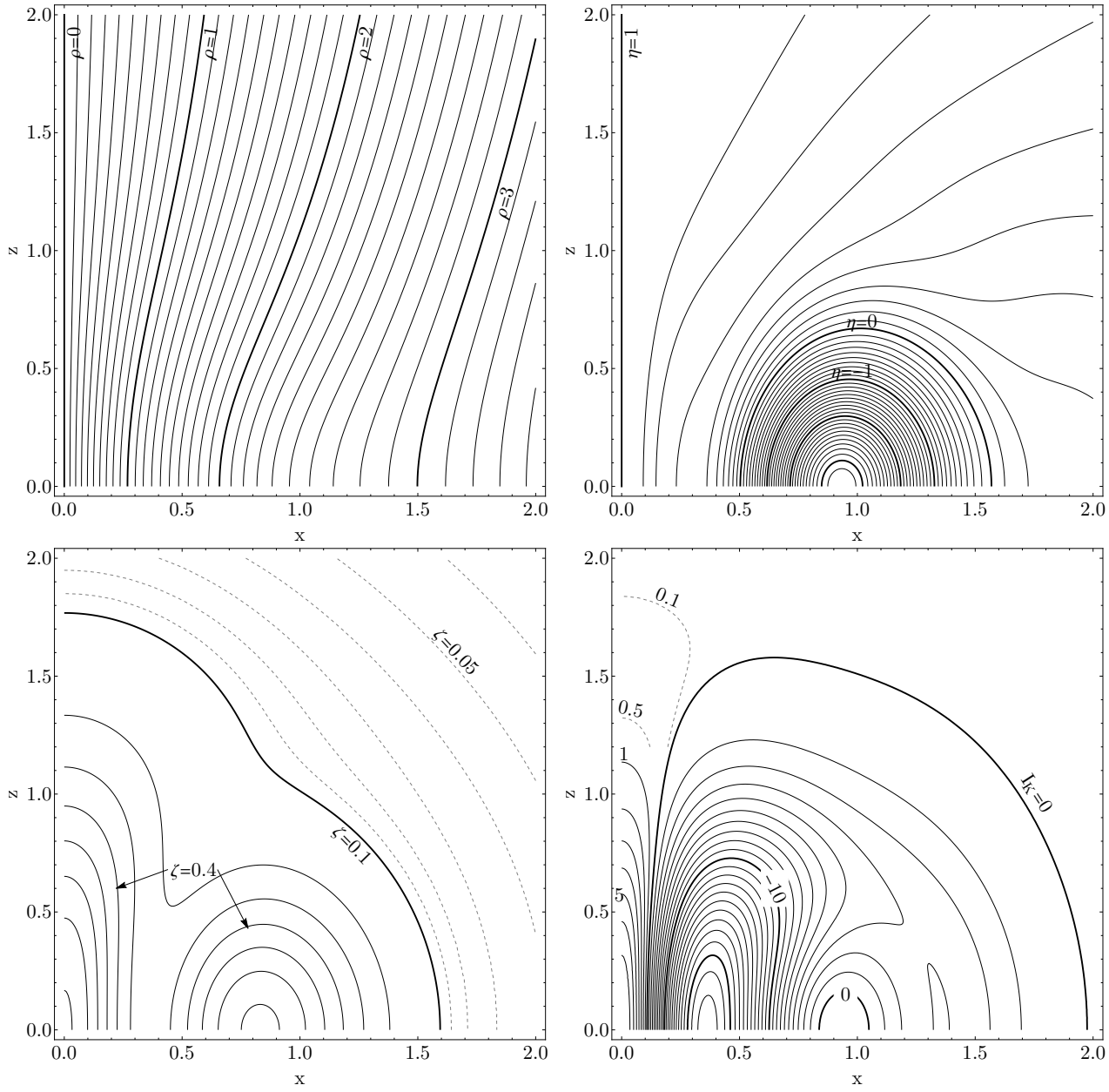

Figure 1.13: Geometry of the initial slice with TA initial data with $\sigma = 1, A^{\rm TA} = \overline{0.9}$ illustrated by the values of spacetime invariants. The TA initial data have γ_{ij} conformally flat and the GW 'seed' appears in K_{ij}. This can be seen in the top plots — the initial K_{ij} makes $\partial_t \rho$ so large, that $\nabla_\alpha \rho$ is time-like ($\eta < 0$). These data are supercritical, see Fig. 1.14. Note that data with $A^{\rm TA} = 0.9$ (without the bar over the number) would be subcritical (see Fig. 1.11).

Black holes born in gravitational-wave collapse

The mathematical certainty which the singularity and horizon theorems [57] provide, can be used as a tool to decide if we observe a black hole in numerical simulation. If we find a marginally outer trapped surface (MOTS), we know that no causal worldline can escape from its interior. (MOTS is a generalization of the spherical photon sphere with constant area made of constant-radius photons mentioned in the description of the Oppenheimer-Snyder collapse.) It represents the so-called apparent horizon in a given slice $t = \text{const}$. To find it, we use a level-function approach [42] with spectral solver and the shooting method we developed for the axisymmetric problem, where MOTS is determined by one curve, its meridian. Such cross-checking is useful, because the former method solves a nonlinear set of equations for spectral coefficients which convergence depends on the initial approximation of the MOTS shape.

For both families, the exponential factor e^{-r^2/σ^2} localizes the seed function on the scale σ. This is also the scale on which the spacetime deviates significantly from the spherically symmetric one (as measured by invariant I_ζ). Because both types of initial data admit an arbitrarily large mass, it is not surprising that there are initial data already containing an apparent horizon [49]. Nevertheless, we will study the collapse of gravitational waves, when it takes some time before a trapped surface 'appears'.

In Fig 1.14 we show a sequence of gravitational field configurations in which the apparent horizon settles to Schwarzschild black hole. We use the quantity ρ to indicate length, ζ as a field-strength indicator and I_ζ which indicates the departure from spherical symmetry. Moreover, for a static Schwarzschild black hole, the horizon coincides with $\zeta = \text{const}$. surface with $\rho^2\zeta = 1$ at the equator. In later times this allows to estimate position of the non-locally defined apparent horizon from the local quantities ζ and ρ.

To get an approximated position of the event horizon, we trace photons back in time from a sufficiently settled apparent horizon. While in the spherically symmetric collapse in Fig. 1.10 the event horizon starts from a single vertex, for axisymmetric gravitational waves the horizon starts along a two-dimensional hypersurface, e.g. in the form of a superluminally expanding ring where photons enter the event horizon and become its generators. This complicates the process of event horizon localization based on partial differential equations [42]. Because the apparent horizon at $t = \text{const}$. hypersurface is not a smooth surface, it excludes a direct application of high-order PDE-solving methods. We thus had to adapt a photon tracing method. In Fig. 1.15 an illustration of the event horizon in the Brill wave collapse simulation is taken from [P5].

Critical behavior

Before we discuss the critical behavior of the axisymmetric GW collapse, we should briefly describe a simpler case of the spherically symmetric scalar field critical collapse. A minimally coupled massless scalar field satisfies the curved spacetime wave equation $\nabla^\mu\nabla_\mu\,\Phi = 0$. Its energy curves spacetime and for spherically symmetric situations there are two generic outcomes of the field evolution — either the field disperses leaving behind the flat Minkowski spacetime or a black hole is created containing some fraction of the total field energy while the remaining field is radiated away. The threshold of black hole formation was numerically studied by Choptuik with a surprising conclusion [40]: If one-parameter family of initial data contains some critical value of this parameter A_* such that for parameter $A < A_*$ the evolution leads to dispersal and for $A > A_*$ a black hole is formed, its mass behaves approximately as $(A - A_*)^\gamma$ where the index γ does not depend on the form of initial data. This universality also included the field which for $A \to A_*$ independently on the shape of the initial data approaches one universal self-similar

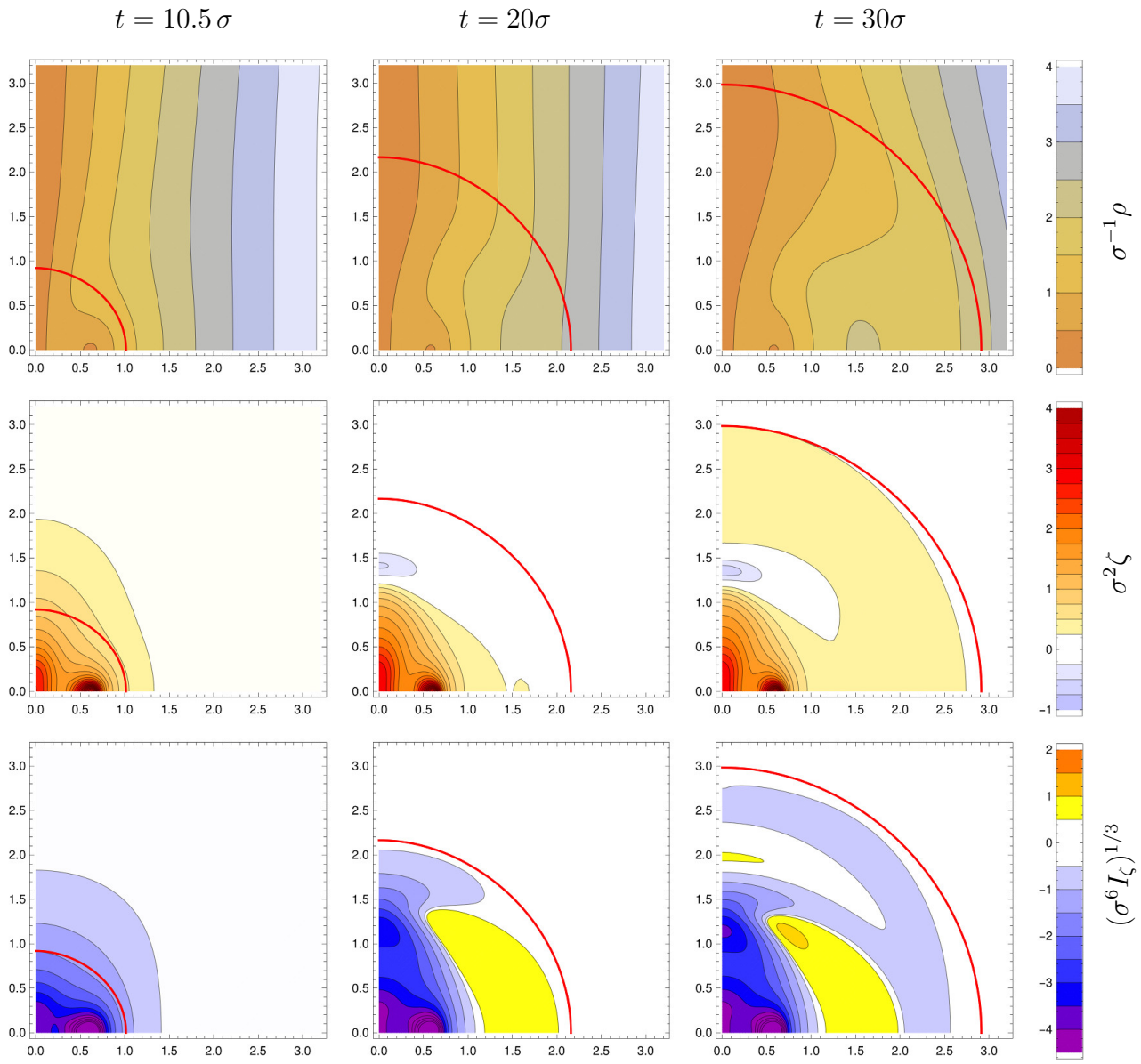

Figure 1.14: Invariant quantities ρ, ζ and I_ζ in the $x-z$ plane as the newly born black hole settles toward the spherically symmetric state in an approximately maximal slicing. TA initial data with $\sigma = 1, A = \overline{0.9}$. The simulation coordinates x, z do not have direct meaning in the central region. Each column shows fields at given simulation time (indicated at the top). The top row shows the circumferential radius ρ and the usual horizon expansion typical for coordinates with $\beta^i = 0$. Red segments indicate MOTS at given times. Notice the difference between coordinate radius and circumferential radius and the fact that all three apparent horizon areas are roughly the same; their masses are $1.03, 1.19, 1.20$, spacetime $M_{\mathrm{ADM}} \doteq 1.24$. The invariant ζ is in the middle row, and I_ζ at the bottom. Departures from the spherically symmetric Schwarzschild geometry are either radiated in the form of gravitational waves or end up inside the black hole. The time slice in the diagrams have very small values of the lapse α farther below horizon, so the evolution and the depicted fields *freeze* near the origin. This saves the simulation from crashing due to infinite curvature of the spacetime singularity.

solution in the central region where the field and metric configuration repeat on ever smaller scales with the ratio of successive scales $e^{-\Delta}$. Later, a similar behavior was observed for many other spherically symmetric field and matter models with different but universal values of the critical parameters γ and Δ for each model (see the review [58]).

Because it was known that a vacuum spacetime can collapse into a black hole if the gravitational waves are highly concentrated [49], the first attempt to study the critical collapse of gravitational waves followed soon after Choptuik's discovery [59]. Nevertheless, after more than two decades of attempts [59, 51, 60, 61, 62, 63, 55], the results of the analysis of the most demanding simulations of GW critical collapse [48] (including also a very detailed review of the previous results) did not find features analogous to the behavior of the critical collapse of the scalar field and showed that important differences exist.

Clearly, the near-critical simulations are complicated by the fact that these simulations need higher resolution as $A \to A_*$. As we mentioned in the Introduction, to admit gravitational waves, we have to assume at most the axial symmetry which requires significantly more computer resources then the spherically symmetric problem.

We localized the critical values A_* of the parameter A for the considered initial data families using standard bisection (see also Fig. 1.11). It turned out that the spacetimes differ significantly between families in the resolution required to keep the slices $t = \text{const.}$ regular.

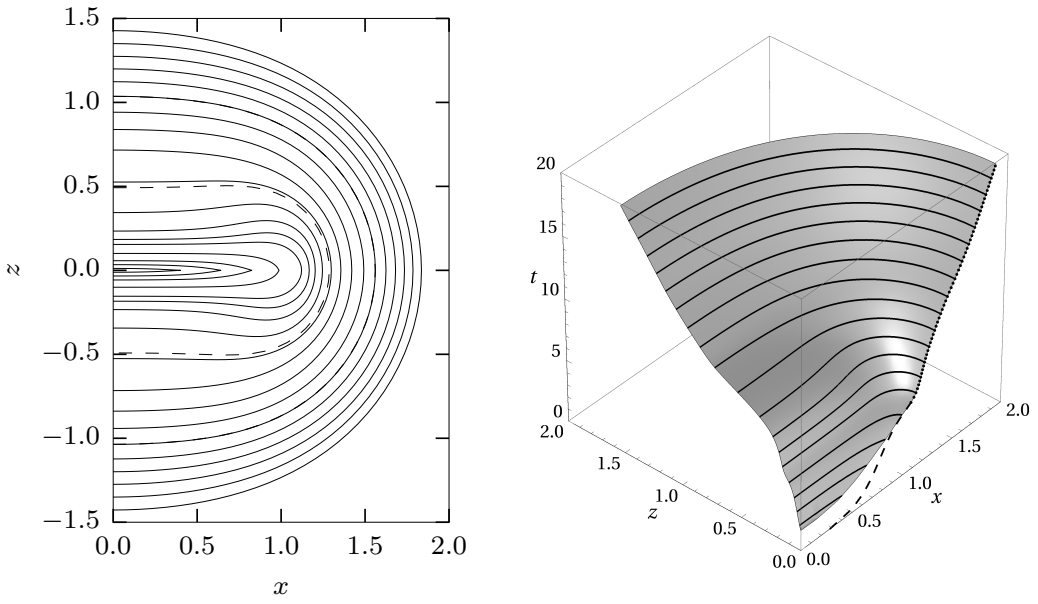

Figure 1.15: *Left:* Event horizon (solid curves) in $x-z$ plane at simulation times $t = 2, 3, ..., 19$ in $\sigma = 1, A^{\text{Brill}} = 5$ simulation with $\beta^i = 0$. The dashed curves show apparent horizon at $t = 10$ (first MOTS appears at $t \approx 9.5$) and $t = 14$ (hardly visible). Much of the horizon growth is a coordinate effect, its area stays almost constant, see Fig. 1.14. The early event horizon is not smooth. It has a rim which worldsheet is a counterpart of the single vertex at the "beginning" of the spherical symmetric event horizon in Fig. 1.10. *Right:* The same plot with added time dimension. It shows that the horizon becomes smooth when null rays propagating radially in the equatorial plane (dashed line) become horizon generators (dotted line). This also shows that at $t = 0$ a photon can escape from the origin along z axis but not in the equatorial plane. Figures are taken from [P5].

Because higher resolution requires larger computational resources, with the most extensive simulations taking $\sim 10^4$ CPU-hours we obtained the critical parameters with varying uncertainty. For TA initial data (1.62) we get critical values of the parameters $A_*^{\mathrm{TA}+} \doteq \overline{1.3008079^{\pm 4}}$, $A_*^{\mathrm{TA}-} \doteq \overline{-1.22434^{\pm 5}}$. (The bar indicates that both values appear on the upper branches of $M_{\mathrm{ADM}}(A)$ dependence shown in Fig. 1.11b.) The Brill initial data (1.60) give the intervals $A_*^{\mathrm{Brill}+} \doteq 4.697^{\pm 1}$ and $A_*^{\mathrm{Brill}-} \doteq -3.509106^{\pm 5}$. The former agrees with much more accurate result $A_*^{\mathrm{Brill}+} \doteq 4.6966953^{\pm 78}$ in [48].

With four different families of initial data, we were able to identify common features as well as differences:

- As expected, as A approaches A_* for subcritical simulations we observe ever larger curvature invariant ζ. For a given simulation, the overall maximum of $|\zeta|$ and $|I_{\mathrm{K}}|$ appears typically at the symmetry axis.

- As A approaches A_* new maxima appear with ever higher amplitude on an ever smaller scale. It is usual to call such features "echoes". These stronger echoes appear later in the simulation than the previous weaker ones and define the overall maximum. The previous "local" extreme is still present in the near-critical simulation as a weaker echo.

- It turned out that from the four initial data families, the most studied $A > 0$ Brill initial data are also the most difficult to evolve near A_*.

- When we estimate the critical exponent in the scaling of the curvature scalar $\max|\zeta| \sim |A - A_*|^{-2\gamma}$ (the form of the exponent is implied by dimension of $[\zeta] = \mathrm{length}^{-2}$) the exponent γ differs significantly between initial data families.

- Unlike in the spherical critical collapse, there seems to be no universality in the echo scale ratios and probably also in the times they appear — they both depend on the initial data family. (We quantify this by appropriately defined scale ratios Δ_ζ and Δ_τ in [P6]. Of course, with four or five echoes it is complicated to say a definitive statement about the limit $A = A_*$.)

- Unlike in the spherical critical collapse, these maxima undergo bifurcation and the second or third one, instead of the coordinate center (which is the center of the reflection symmetry of our problem), a pair of maxima appears on the z-axis symmetrically arranged with respect to $z = 0$.

- When the parameter A approaches the critical value in the supercritical regime, close-enough to A_* we can detect a pair of black holes before they merge into a common apparent horizon. (We reached the necessary resolution only with Brill $A > 0$ (see also [48]) and for TA $A > 0$ initial data.

- We observe an approximate self-similarity of the 1+1 $z-t$ submanifold. We demonstrate it so that we construct the dimensionless quantity $\hat{\zeta} = (\tau - \tau_*)^2\zeta$. For an exactly self-similar critical spacetime, we can first define τ as a proper time along the central worldline $x^i \equiv 0$ an then distribute it in some geometrically covariant way into $x^i \neq 0$ denoting τ_* the τ of the $A = A_*$ critical spacetime accumulation event. Then $\hat{\zeta}$ is manifestly discretely self-similar $\hat{\zeta}(te^{n\Delta}, x^i\, e^{n\Delta}) = \hat{\zeta}(t, x^i)$ with $n = 0, 1, 2, ...$ The approximate self-similarity of the gravitational wave near-critical spacetime is then demonstrated in [P6]. The main argument is based on the observation, that while maxima of ζ in a near-critical spacetime

differ by factor > 400 using the quantity $\hat{\zeta}$ this factor drops to ~ 3. This allowed us to plot color-coded function values of $\hat{\zeta}$ in Fig. 1.17. We find that this "dimensionless curvature" is $10^2 - 10^3$ times larger than for the scalar field, indicating the principally different nature of the effects observed.

- We were able to demonstrate a universal form of the echo time profiles. Because the quantity ζ is not dimensionless, we first determine the scale λ^{-1} from the echo amplitude, $\lambda = \sqrt{2/|\zeta_{\min}|}$. We then plot the rescaled time dependence $\zeta_0(\tau_0) \equiv \lambda^2\zeta(t = t_e + \lambda\tau_0, z = z_e)$ for the curvature invariant ζ along an approximate geodesic passing through the event $t = t_e, z = z_e$ of the extreme ζ. In Fig. 1.16 taken from [P6] we demonstrate the universality of these rescaled profiles.

Although we found that the scaling exponent γ is not universal, a detailed explanation of this phenomenon is missing. To construct more-dimensional counterpart of Fig. 1.16 we have to find an appropriate method, because the numerical evolution covers these patches by different coordinates. Since the lower symmetry of the problem leaves a much richer space of collapse outcomes than in the spherical symmetry, there remain many other open questions.

Because there exists only one nontrivial component of the curvature tensor on the axis of an axisymmetric vacuum spacetime, the observed universality means that the echoes represent ever smaller copies of a piece of some particular spacetime. Its properties have yet to be understood, nevertheless in the neighborhood of the echo maximum, the spacetime is in some aspects similar to the classical model of the cylindrically symmetric gravitational wave introduced in 1957 by Weber and Wheeler [65] to demonstrate "Reality of the Cylindrical Gravitational Waves of Einstein and Rosen".

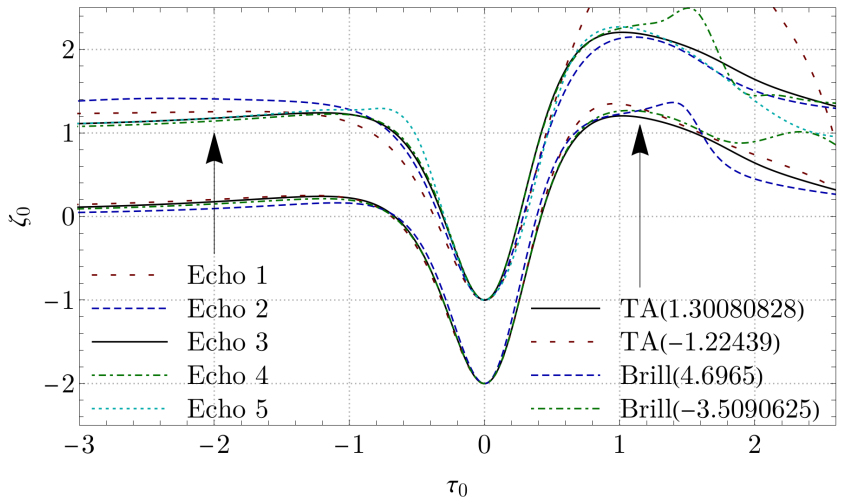

Figure 1.16: Profiles of the invariant ζ along a timelike worldline through 'echo' when rescaled in time and amplitude, i.e., $\zeta_0 = \lambda^2\zeta(\tau_e + \lambda\tau_0)$ (see text). The same scale λ is chosen so that we get dimensionless both the function value and the argument and so that at the minimum we get $\min(\zeta_0) = -2$. *Top curves* show the shifted value $\zeta_0 + 1$ of five successive 'echoes' which appear in the simulation with initial data (1.62) with $A_{\mathrm{TA}^+} = \overline{1.30080828}$. To demonstrate the universality of the curvature spikes, the *bottom curves* compare the observed profiles of ζ_0 of four different families of initial data with indicated initial data parameters. The plot is taken from [P6].

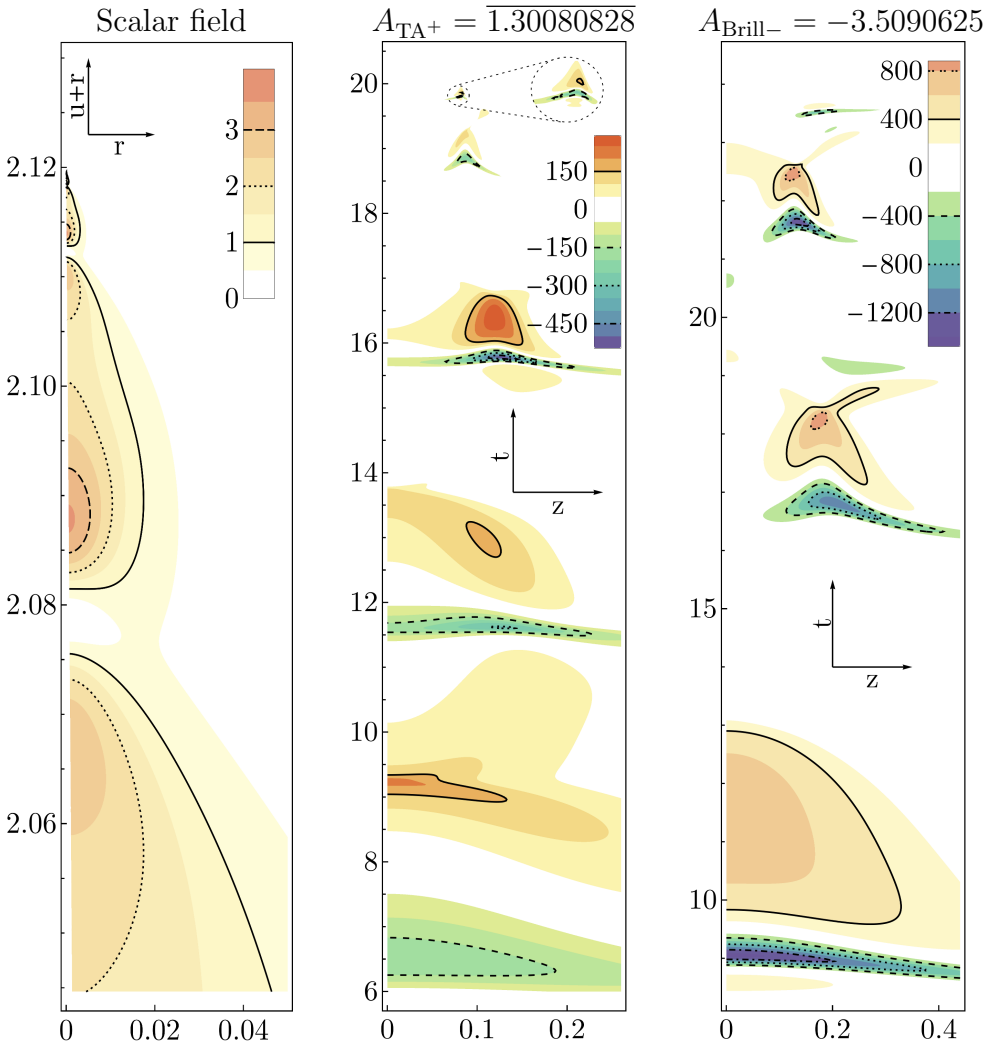

Figure 1.17: *Left:* The near-critical solution for the spherically symmetric collapse of the scalar field approaches a universal discretely self-symmetric critical solution. A dimensionless quantities then demonstrate this by acquiring repeatedly the same values on ever smaller scales. The dimensionless quantity $\hat{\zeta} = (\tau - \tau_*)^2\zeta$ is shown in all three spacetime diagrams. For the scalar field critical collapse in the left panel, τ is the proper time at the center of spherical symmetry extended into the whole spacetime. For the exactly critical spacetime infinitely small echoes with diverging curvature appear in the center at $\tau = \tau_*$. Our scalar field simulations followed methods, coordinates, and initial data described in Ref. [64]. *Middle:* In the near-critical evolution of collapsing gravitational waves, small regions of high spacetime curvature (echoes) appear off the center. We measure the proper time τ along worldline through this center and then extend τ along our approximately maximal slices $t = \text{const}$. Thus, $\hat{\zeta}$ is a coordinate dependent quantity. The accumulation point proper time τ_* is estimated. When plotted in a color-coded graph, $\hat{\zeta}$ illustrates approximate self-similarity of the echo regions. Results of a simulation with five echoes are shown. *Right:* Evolution of the near-critical $A < 0$ Brill initial data. Despite the similarity with the TA simulation, the plotted $\hat{\zeta}$ has significantly larger amplitude. Thus, while for the scalar field (left), the quantity $\hat{\zeta}$ is universal across various initial data families, in GW collapse, although we observe universal time profile of echoes (Fig. 1.16), the echoes appear irregularly and thus the amplitude of $\hat{\zeta}$ varies among initial data families. For further details see [P6].

Bibliography

[1] G. Schäfer and P. Jaranowski. "Hamiltonian formulation of general relativity and post-Newtonian dynamics of compact binaries". *Living Reviews in Relativity* 21, 1 (2018), 7.

[2] R. Arnowitt, S. Deser, and C. Misner. "The dynamics of general relativity". In: *Gravitation an introduction to current research*. Ed. by L. Witten. John Wiley, New York, 1962, 227.

[3] B. S. DeWitt. "Quantum Theory of Gravity. I. The Canonical Theory". *Physical Review* 160, 5 (1967), 1113.

[4] D. R. Brill and R. W. Lindquist. "Interaction Energy in Geometrostatics". *Physical Review* 131, 1 (1963), 471.

[5] G. Schäfer. "The ADM Hamiltonian at the postlinear approximation." *General Relativity and Gravitation* 18, 3 (1986), 255.

[6] J. D. Jackson. *Classical Electrodynamics*. 3rd. John Wiley & Sons, Inc., 2002.

[7] P. Jaranowski and G. Schäfer. "Third post-Newtonian higher order ADM Hamilton dynamics for two-body point-mass systems". *Phys. Rev. D* 57, 12 (1998), 7274.

[8] T. Damour, P. Jaranowski, and G. Schäfer. "Poincaré invariance in the ADM Hamiltonian approach to the general relativistic two-body problem". *Phys. Rev. D* 62, 2 (2000), 021501.

[9] T. Damour, P. Jaranowski, and G. Schäfer. "Erratum: Poincaré invariance in the ADM Hamiltonian approach to the general relativistic two-body problem [Phys. Rev. D 62, 021501(R) (2000)]". *Phys. Rev. D* 63, 2 (2000), 029903.

[10] L. Bernard et al. "Center-of-mass equations of motion and conserved integrals of compact binary systems at the fourth post-Newtonian order". *Phys. Rev. D* 97, 4 (2018), 044037.

[11] A. Lecke, R. Steinbauer, and R. Švarc. "The regularity of geodesics in impulsive pp-waves". *General Relativity and Gravitation* 46 (2014), 1648.

[12] G. Kälin, Z. Liu, and R. A. Porto. "Conservative Dynamics of Binary Systems to Third Post-Minkowskian Order from the Effective Field Theory Approach". *Phys. Rev. Lett.* 125, 26 (2020), 261103.

[13] Z. Bern et al. "Scattering Amplitudes and Conservative Binary Dynamics at O (G^4)". *Phys. Rev. Lett.* 126, 17 (2021), 171601.

[14] G. U. Jakobsen et al. "Classical Gravitational Bremsstrahlung from a Worldline Quantum Field Theory". *Phys. Rev. Lett.* 126, 20 (2021), 201103.

[15] T. Damour and R. Ruffini. "Analisi di un gruppo omogeneo di occultazioni lunari totali." *Academie des Sciences Paris Comptes Rendus Serie Sciences Mathematiques* 279, 26 (1974), 971.

[16] B. M. Barker and R. F. O'Connell. "Gravitational two-body problem with arbitrary masses, spins, and quadrupole moments". *Phys. Rev. D* 12, 2 (1975), 329.

[17] J. Steinhoff, G. Schäfer, and S. Hergt. "ADM canonical formalism for gravitating spinning objects". *Phys. Rev. D* 77, 10 (2008), 104018.

[18] E. Barausse, E. Racine, and A. Buonanno. "Hamiltonian of a spinning test particle in curved spacetime". *Phys. Rev. D* 80, 10 (2009), 104025.

[19] M. Mathisson. "Republication of: New mechanics of material systems". *General Relativity and Gravitation* 42, 4 (2010), 1011.

[20] A. Papapetrou. "Spinning Test-Particles in General Relativity. I". *Proceedings of the Royal Society of London Series A* 209, 1097 (1951), 248.

[21] W. G. Dixon. "Dynamics of Extended Bodies in General Relativity. I. Momentum and Angular Momentum". *Proceedings of the Royal Society of London Series A* 314, 1519 (1970), 499.

[22] K. Kyrian and O. Semerák. "Spinning test particles in a Kerr field - II". *Mon. Not. R. Astron. Soc.* 382, 4 (2007), 1922.

[23] L. F. O. Costa and J. Natário. "Center of Mass, Spin Supplementary Conditions, and the Momentum of Spinning Particles". In: *Equations of Motion in Relativistic Gravity.* 2015, 215.

[24] B. Carter. "Global Structure of the Kerr Family of Gravitational Fields". *Physical Review* 174, 5 (1968), 1559.

[25] J. Vines et al. "Canonical Hamiltonian for an extended test body in curved spacetime: To quadratic order in spin". *Phys. Rev. D* 93, 10 (2016), 103008.

[26] J. B. Barbour and H. Pfister, eds. *Mach's Principle: From Newton's Bucket to Quantum Gravity.* Boston: Birkhäuser, 1995.

[27] D. Lindblom L. and Brill. "Inertial effects in the gravitational collapse of a rotating shell". *Phys. Rev. D* 10 (1974), 3151.

[28] D. Lynden-Bell, J. Bičák, and J. Katz. "Inertial frame rotation induced by rotating gravitational waves". *Class. Quantum Grav.* 25 (2008), 165018.

[29] T. Regge and J. A. Wheeler. "Stability of a Schwarzschild Singularity". *Physical Review* 108, 4 (1957), 1063.

[30] R. A. Isaacson. "Gravitational Radiation in the Limit of High Frequency. I. The Linear Approximation and Geometrical Optics". *Physical Review* 166, 5 (1968), 1263.

[31] F. J. Zerilli. "Gravitational Field of a Particle Falling in a Schwarzschild Geometry Analyzed in Tensor Harmonics". *Phys. Rev. D* 2, 10 (1970), 2141.

[32] H. Nakano and K. Ioka. "Second-order quasinormal mode of the Schwarzschild black hole". *Phys. Rev. D* 76, 8 (2007), 084007.

[33] J. Bicak. "On the theories of the interacting perturbations of the Reissner-Nordström black hole." *Czechoslovak Journal of Physics* 9 (1979), 945.

[34] K. S. Thorne. "Multipole expansions of gravitational radiation". *Reviews of Modern Physics* 52, 2 (1980), 299.

[35] J. Weber and J. A. Wheeler. "Reality of the Cylindrical Gravitational Waves of Einstein and Rosen". *Rev. Mod. Phys.* 29, 3 (1957), 509.

[36] C. Montgomery, W. Orchiston, and I. Whittingham. "Michell, Laplace and the origin of the black hole concept". *Journal of Astronomical History and Heritage* 12, 2 (2009), 90.

[37] J. R. Oppenheimer and H. Snyder. "On Continued Gravitational Contraction". *Physical Review* 56, 5 (1939), 455.

[38] R. Penrose. "Singularity theorems". In: *Topology and Physics*. Ed. by C. N. Yang, M.-L. Ge, and Y.-H. He. Singapore: World Scientific, 2019. Chap. 5, 135.

[39] R. Penrose. "The Question of Cosmic Censorship". *Journal of Astrophysics and Astronomy* 20 (1999), 233.

[40] M. W. Choptuik. "Universality and scaling in gravitational collapse of a massless scalar field". *Phys. Rev. Lett.* 70, 1 (1993), 9.

[41] F. Löffler et al. "The Einstein Toolkit: a community computational infrastructure for relativistic astrophysics". *Classical and Quantum Gravity* 29, 11 (2012), 115001.

[42] T. W. Baumgarte and S. L. Shapiro. *Numerical Relativity: Solving Einstein's Equations on the Computer*. 2010.

[43] O. A. Reula. "Hyperbolic Methods for Einstein's Equations". *Living Reviews in Relativity* 1, 1 (1998), 3.

[44] T. W. Baumgarte and S. L. Shapiro. "On the numerical integration of Einstein's field equations". *Phys. Rev. D* 59 (1999), 024007.

[45] M. Shibata and T. Nakamura. "Evolution of three-dimensional gravitational waves: Harmonic slicing case". *Phys. Rev. D* 52, 10 (1995), 5428.

[46] J. D. Brown et al. "Turduckening black holes: an analytical and computational study". *Phys. Rev. D* 79 (2009), 044023.

[47] J. Winicour. "Characteristic Evolution and Matching". *Living Reviews in Relativity* 12, 1 (2009), 3.

[48] D. Hilditch, A. Weyhausen, and B. Brügmann. "Evolutions of centered Brill waves with a pseudospectral method". *Phys. Rev. D* 96, 10 (2017), 104051.

[49] K. Eppley. "Evolution of time-symmetric gravitational waves: Initial data and apparent horizons". *Phys. Rev. D* 16, 6 (1977), 1609.

[50] D. R. Brill. "On the positive definite mass of the Bondi-Weber-Wheeler time-symmetric gravitational waves". *Annals of Physics* 7, 4 (1959), 466.

[51] A. M. Abrahams and C. R. Evans. "Universality in axisymmetric vacuum collapse". *Phys. Rev. D* 49, 8 (1994), 3998.

[52] J. P. Boyd. *Chebyshev and Fourier Spectral Methods*. Dover Publications Inc., New York, 2001.

[53] M. Campanelli et al. "Accurate Evolutions of Orbiting Black-Hole Binaries without Excision". *Phys. Rev. Lett.* 96, 11 (2006), 111101.

[54] C. Bona et al. "New Formalism for Numerical Relativity". *Phys. Rev. Lett.* 75, 4 (1995), 600.

[55] D. Hilditch et al. "Collapse of nonlinear gravitational waves in moving-puncture coordinates". *Phys. Rev. D* 88, 10 (2013), 103009.

[56] H. Stephani et al. *Exact solutions of Einstein's field equations; 2nd ed.* Cambridge: Cambridge Univ. Press, 2003.

[57] S. W. Hawking and G. F. R. Ellis. *The Large Scale Structure of Space-Time*. 1975.

[58] C. Gundlach. "Critical Phenomena in Gravitational Collapse". *Living Reviews in Relativity* 2, 1 (1999), 4.

[59] A. M. Abrahams and C. R. Evans. "Critical behavior and scaling in vacuum axisymmetric gravitational collapse". *Phys. Rev. Lett.* 70, 20 (1993), 2980.

[60] M. Alcubierre et al. "Gravitational collapse of gravitational waves in 3D numerical relativity". *Phys. Rev. D* 61, 4 (2000), 041501.

[61] D. Garfinkle and G. C. Duncan. "Numerical evolution of Brill waves". *Phys. Rev. D* 63, 4 (2001), 044011.

[62] O. Rinne. "Constrained evolution in axisymmetry and the gravitational collapse of prolate Brill waves". *Classical and Quantum Gravity* 25, 13 (2008), 135009.

[63] E. Sorkin. "On critical collapse of gravitational waves". *Classical and Quantum Gravity* 28, 2 (2011), 025011.

[64] M. Pürrer, S. Husa, and P. C. Aichelburg. "News from critical collapse: Bondi mass, tails, and quasinormal modes". *Phys. Rev. D* 71, 10 (2005), 104005.

[65] J. Weber and J. A. Wheeler. "Reality of the Cylindrical Gravitational Waves of Einstein and Rosen". *Reviews of Modern Physics* 29, 3 (1957), 509.

List of acronyms

ADM	Arwnowitt-Deser-Misner	Page 10
CMS	Ceter of Mass System	Page 15
GW	Gravitational Wave	Page 20
MOTS	Marginally Outer Trapped Surface	Page 39
PDE	Partial Differential Equation	Page 32
PM	Post-Minkowskian	Page 11
PN	Post-Newtonian	Page 9
QMS	Quasi-Maximal Slicing	Page 36
SSC	Spin Supplementary Condition	Page 17
TA	Time-Asymmetric	Page 34
TT	Transverse-Traceless	Page 10
ZAMO	Zero Angular Momentum Observer	Page 18

Chapter 2

Selected original papers

List of selected original papers

[P1] T. Ledvinka, G. Schäfer, J. Bičák, Relativistic closed-form Hamiltonian for many-body gravitating systems in the post-Minkowskian approximation, *Physical Review Letters*, vol. 100, no. 25 (2008), p. 251101. DOI 10.1103/PhysRevLett.100.251101.

[P2] D. Kunst, T. Ledvinka, G. Lukes-Gerakopoulos, J. Seyrich, Comparing Hamiltonians of a spinning test particle for different tetrad fields, *Physical Review D*, vol. 93, no. 4 (2016), p. 044004. DOI 10.1103/PhysRevD.93.044004.

[P3] J. Bičák, J. Katz, T. Ledvinka, D. Lynden-Bell, Effects of rotating gravitational waves, *Physical Review D*, vol. 85, no. 12 (2012), p. 124003. DOI 10.1103/PhysRevD.85.124003.

[P4] W. Barker, T. Ledvinka, D. Lynden-Bell, J. Bičák, Rotation of inertial frames by angular momentum of matter and waves, *Classical and Quantum Gravity*, vol. 34, no. 20 (2017), p. 205006. DOI 10.1088/1361-6382/aa8a34.

[P5] A. Khirnov, T. Ledvinka, Slicing conditions for axisymmetric gravitational collapse of Brill waves, *Classical and Quantum Gravity*, vol. 35, no. 21 (2018), p. 215003. DOI 10.1088/1361-6382/aae1bc.

[P6] T. Ledvinka, A. Khirnov, Universality of Curvature Invariants in Critical Vacuum Gravitational Collapse, *Physical Review Letters*, vol. 127, no. 1 (2021), p. 011104. DOI 10.1103/PhysRevLett.127.011104.